THE ASTROPHYSICAL JOURNAL, 421:178–194, 1994 January 20

ON THE ELLIPTICITY OF THE GALACTIC DISK

KONRAD KUIJKEN
Harvard-Smithsonian Center for Astrophysics, 60 Garden Street, Cambridge, MA 02138. E-mail: kuijken@cfa.harvard.edu
AND
SCOTT TREMAINE
Canadian Institute for Theoretical Astrophysics, University of Toronto, 60 St. George Street, Toronto, Ontario, Canada M5S 1A7.
E-mail: tremaine@cita.utoronto.ca
Received 1993 January 22; accepted 1993 July 30

ABSTRACT

We investigate two kinds of constraints on the ellipticity of the Galactic disk: local constraints, based on the kinematics of the solar neighborhood (such as the Oort constants, the axis ratio of the velocity ellipsoid, the vertex deviation, and the radial velocity of the local standard of rest relative to the Galactic center), and global constraints (H I tangent point velocities, the velocity fields of distant carbon stars, Cepheids, and H II regions, and the kinematics of distant H I). Local and global constraints independently suggest that the Sun lies near the minor axis of the potential of an elliptical Galactic disk, with equipotential axis ratio 0.9. The kinematic data are consistent with a flat rotation curve of constant ellipticity, with a mean rotation speed of 200 km s^{-1}. In this model, the present velocity of the local standard of rest is 180 km s^{-1}.

Subject headings: Galaxy: fundamental parameters — Galaxy: halo — Galaxy: kinematics and dynamics — Galaxy: structure — solar neighborhood

1. INTRODUCTION

Most astronomers believe that disk galaxies are surrounded by massive unseen halos. If these halos form through dissipationless collapse of primordial density fluctuations, few of them should be round; rather, a typical galactic halo is expected to be strongly triaxial (e.g., Dubinski & Carlberg 1991), although triaxial halos tend to become oblate under the uncertain influence of dissipation in the gaseous component of the collapsing galaxy (Katz & Gunn 1991).

The shapes of orbits in the disk are influenced by the halo potential: in particular, if the disk lies in a principal plane of a triaxial halo then we expect the closed orbits in the disk to be elliptical. Binney (1978) was the first to consider the effects of triaxial halos surrounding disk galaxies, showing that they might explain the observed warps and apparent twists seen in many disks. Kuijken & Tremaine (1991, hereafter KT) used halo parameters taken from Dubinski & Carlberg's (1991) simulations to estimate that the disk axis ratio q at 15 kpc in a typical galaxy should be given by $1 - q \approx 0.1$.

The distribution of axis ratios of nearby disk galaxies can be estimated from the distribution of apparent ellipticities and inclinations (determined from the Tully-Fisher relation) or of differences between photometric and kinematic position angles and inclinations (KT; Franx & de Zeeuw 1992). The data indicate that typically $1 - q \approx 0.1$, although with considerable uncertainty and possible systematic biases that tend to increase the apparent ellipticity. Franx and de Zeeuw have argued that the scatter in the Tully-Fisher relation for disk galaxies sets an upper limit $1 - q \lesssim 0.1$. They also argue that ellipticity is unlikely to be the sole source of the "cosmic" scatter in the Tully-Fisher relation, and suggest that, on average, $1 - q \lesssim 0.06$.

The observational data on the shapes of halos is as modest as the data on the shapes of disks. The flaring of H I disks at large radii, the spherical distribution of tracers such as globular clusters, and the similarity of the rotation curves of polar rings and equatorial disks all suggest that halos are "more nearly spherical than flat" (in the words of Kormendy's 1988 review), but do not constrain halo triaxiality at the level we are considering here. A more recent investigation by Sackett & Sparke (1990) of the polar ring galaxy NGC 4650A concluded that the halo has a polar flattening between E3 and E7. All of these observational constraints are on flattening and do not address the likely deviations from axisymmetry in dark halos.

In this paper, we will examine the evidence for nonaxisymmetric distortions in the disk of our own Galaxy. We shall focus on nonrotating elliptical distortions such as might be caused by a triaxial halo, although many of our methods and conclusions are also relevant to more general distortions.

The detection of nonaxisymmetric distortions in our Galaxy is difficult, in part because the Sun lies within the disk. The most obvious signature of such a distortion is asymmetry between Galactic longitudes l and $-l$. The difficulty of detecting a distortion increases substantially when the Sun lies near a symmetry axis of the distortion, because then there are no asymmetries between positive and negative longitudes. In fact we shall argue that this is the case: that there is a significant distortion of the disk, of about the magnitude expected from the theoretical and observational arguments above, that has not been obvious simply because the Sun happens to lie near a symmetry axis. More generally, an arbitrary small distortion can be decomposed into "even" and "odd" components, in which the potential and density are even and odd, respectively, under reflection through a plane containing the Sun, Galactic center, and Galactic poles. Most of our discussion is directed toward constraining the even component, which has received little or no attention in the literature so far.

After reviewing the dynamical consequences of an elliptical distortion in § 2 we will concentrate on two basic kinds of observation that can be used to probe for distortions:

1. Local observations, based on the kinematics in the solar neighborhood (§ 3). These included the Oort constants C and

K, the velocity of the local standard of rest along the Sun-Galactic center line, and the shape and orientation of the velocity ellipsoid.

2. Global observations, based on the kinematics of distant objects, mostly between the solar radius R_0 and $2R_0$ (§ 4). The tracers we will discuss include H I, H II regions, carbon stars, and Cepheids.

More details on some of this work are described in KT.

1.1. *Notation*

Throughout this paper, we employ polar coordinates (R, ϕ) in the Galactic plane, with $R = 0$ at the Galactic center. The Sun is at $(R_0, \phi = 0)$, and ϕ is measured in the direction of Galactic rotation. The usual Galactic longitude is denoted by l. Motions perpendicular to the Galactic plane will be ignored. The local standard of rest (LSR) is the frame in which the mean velocity of the stars in the solar neighborhood, corrected for asymmetric drift, is zero. We use $f_{,x}$ as shorthand for $\partial f/\partial x$. Bars denote averages over all stars at a given position; thus $\bar{\boldsymbol{v}}(\boldsymbol{x})$ is the mean velocity at position $\boldsymbol{x}$.

2. A SIMPLE MODEL OF AN ELLIPTICAL DISK

We consider the potential

$$\Psi(R, \phi) = \Psi_0(R) + \psi(R) \cos 2(\phi - \phi_b) , \tag{1}$$

where ϕ_b is a constant. The axisymmetric part of the potential is chosen to yield a power-law rotation curve $v_{\rm circ}(R) = (R/R_0)^{\alpha} v_c$, where v_c is the circular speed in the solar neightborhood:

$$\begin{aligned} \Psi_0(R) = \frac{v_c^2}{2\alpha}\left(\frac{R}{R_0}\right)^{2\alpha} \quad & \text{if} \quad \alpha \neq 0 , \\ \text{or} \quad v_c^2 \ln(R) \quad & \text{if} \quad \alpha = 0 ; \end{aligned} \tag{2}$$

the nonaxisymmetric potential (assumed small) is stationary in an inertial frame and has twofold symmetry, which are appropriate assumptions if the potential arises from a triaxial halo. This potential is also chosen to be a power law in radius:

$$\psi(R) = \psi_0 (R/R_0)^p , \quad \psi_0 \geq 0 . \tag{3}$$

Plausible values of p range from -3 (for a bar or triaxial bulge located well inside the solar circle) to $+2$ (for a halo with core radius much larger than the solar circle). The equipotential surfaces are approximately elliptical, with axis ratio $q_\Psi \equiv 1 - \epsilon_\Psi + O(\epsilon_\Psi^2)$, where

$$\epsilon_\Psi(R) = \frac{2\psi(R)}{v_{\rm circ}^2(R)} . \tag{4}$$

Since $\psi(R)$ is positive, $\phi = \phi_b$ is the minor axis of the potential. More general perturbations (including nonstationary potentials as well as potentials with different azimuthal wavenumbers) are discussed in KT. For a cold (low-velocity dispersion) population, the mean velocity at (R, ϕ) in the potential (1) can be shown to be $\bar{\boldsymbol{v}}(R, \phi) = \bar{v}_R \boldsymbol{e}_R + \bar{v}_\phi \boldsymbol{e}_\phi + O(\epsilon_\Psi^2)$, where (KT, eq. [20])

$$\bar{v}_R = -\left(\frac{1 + \frac{1}{2}p}{1 - \alpha}\right)\epsilon_\Psi v_{\rm circ} \sin 2(\phi - \phi_b) ; \tag{5a}$$

$$\bar{v}_\phi = v_{\rm circ} - \left[\frac{1 + \frac{1}{4}p(1 + \alpha)}{1 - \alpha}\right]\epsilon_\Psi v_{\rm circ} \cos 2(\phi - \phi_b) . \tag{5b}$$

The mean velocity field near the Sun can be expanded in powers of the distance r from the Sun, to yield mean line-of-sight velocities $\bar{v}_{\rm los}$ and proper motions $\bar{\mu}$ relative to the LSR:

$$\begin{aligned} \bar{v}_{\rm los} &= r(K + A \sin 2l + C \cos 2l) + O(r^2) ; \\ \bar{\mu} &= B + A \cos 2l - C \sin 2l + O(r) . \end{aligned} \tag{6}$$

In an axisymmetric, stationary disk, $C = K = 0$ and A and B are the usual Oort constants,

$$\begin{aligned} A = A_{\rm axi} &\equiv \tfrac{1}{2}(v_{\rm circ}/R - v_{{\rm circ},R})_{R_0} , \\ B = B_{\rm axi} &\equiv -\tfrac{1}{2}(v_{\rm circ}/R + v_{{\rm circ},R})_{R_0} . \end{aligned} \tag{7}$$

In a more general velocity field, we have (KT, eq. [13])

$$\begin{aligned} 2A &= \bar{v}_\phi/R - \bar{v}_{R,\phi}/R - \bar{v}_{\phi,R} , \\ 2B &= -\bar{v}_\phi/R + \bar{v}_{R,\phi}/R - \bar{v}_{\phi,R} , \\ 2C &= -\bar{v}_R/R - \bar{v}_{\phi,\phi}/R + \bar{v}_{R,R} , \\ 2K &= \bar{v}_R/R + \bar{v}_{\phi,\phi}/R + \bar{v}_{R,R} , \end{aligned} \tag{8}$$

all evaluated at $R = R_0$. For the elliptical potential (1) we have from equation (5)

$$\begin{aligned} A &= A_{\rm axi} + \frac{\epsilon_\Psi v_c}{2R_0} \\ &\quad \times \frac{1 - \alpha + \frac{1}{4}p[7 - 2\alpha - \alpha^2 + p(1 + \alpha)]}{1 - \alpha} \cos 2(\phi - \phi_b) ; \\ B &= B_{\rm axi} - \frac{\epsilon_\Psi v_c}{2R_0} \\ &\quad \times \frac{1 + \alpha - \frac{1}{4}p[1 - \alpha^2 + p(1 + \alpha)]}{1 - \alpha} \cos 2(\phi - \phi_b) ; \\ C &= -\frac{\epsilon_\Psi v_c}{2R_0}\frac{1 - \alpha + p(1 + \frac{1}{2}p)}{1 - \alpha} \sin 2(\phi - \phi_b) ; \\ K &= \frac{\epsilon_\Psi v_c}{2R_0}\frac{1 + \alpha(1 + p) - p(1 + \frac{1}{2}p)}{1 - \alpha} \sin 2(\phi - \phi_b) , \end{aligned} \tag{9}$$

with errors $O(\epsilon_\Psi^2)$.

The distribution of residual velocities (velocities of stars relative to the local mean velocity) is described by the velocity-dispersion tensor $\sigma_{ij} = \overline{(v_i - \bar{v}_i)(v_j - \bar{v}_j)}$, or equivalently by the velocity ellipsoid, which is an imaginary surface given by $x_i \sigma_{ij}^{-1} x_j = 1$. Apart from a scale factor, the planar components of the velocity-dispersion tensor are specified by two parameters: the vertex deviation l_v (the Galactic longitude of the long axis of the velocity ellipsoid), and the axis ratio X, given by $X^2 \equiv \sigma_{\phi\phi}/\sigma_{RR}$. In an axisymmetric, stationary disk, the vertex deviation l_v is zero and furthermore, provided the velocity dispersions are sufficiently small, X is determined by the Oort constants:

$$X^2 = \frac{-B_{\rm axi}}{A_{\rm axi} - B_{\rm axi}} = \frac{(Rv_{\rm circ})_{,R}}{2v_{\rm circ}}\bigg|_{R=R_0} = \frac{1 + \alpha}{2} . \tag{10}$$

For a flat rotation curve, this relation predicts $X^2 = \frac{1}{2}$. Unfortunately, "sufficiently small" barely applies in the solar neighborhood: even when $\sigma_{RR} \simeq 0.04 v_c^2$, a typical value for an old

disk population, corrections arising from radial gradients in stellar density and velocity dispersion can (and do) spoil the validity of this relation.[1] For example, if we model the Galactic disk as having a constant circular speed, with surface density Σ and radial velocity dispersion satisfying

$$\Sigma(R) \propto \sigma_{RR} \propto e^{-R/h} \tag{11}$$

(as suggested by observations of our own and other disk galaxies), the predicted axis ratio is given by (KT, eq. [6])

$$X^2 = X_0^2 \equiv \tfrac{1}{2} + (\tfrac{5}{4}\xi^2 - \xi - \tfrac{1}{8})b + O(b^2)\,, \tag{12}$$

where $b = \sigma_{RR}/v_c^2$ and $\xi = R/h$. Local values for old disk stars are $b = 0.03$–0.04, $\xi = 2$–2.5, which implies $X_0^2 = 0.66 \pm 0.06$: the correction to the leading-order prediction $X^2 = \frac{1}{2}$ can thus be as large as 40%. In spite of this complication, it will turn out that observations of X are of considerable interest for our study of the disk ellipticity.

An elliptical potential of the form (1) with $|\epsilon_\Psi| \ll 1$ will produce the following vertex deviation and axis ratio perturbation (KT, eqs. [19] and [27]):

$$l_v = \frac{(2+p)[4+(1+\alpha)(3p-2\alpha)]}{4(1-\alpha)^2(1+2\alpha)}\,\epsilon_\Psi \sin 2(\phi-\phi_b)\,; \tag{13a}$$

$$\frac{\delta X^2}{X_0^2} = -\frac{3(1-\alpha)+p(2+\alpha)(2+\frac{1}{2}p-\alpha)}{(1-\alpha)(1+2\alpha)} \times \epsilon_\Psi \cos 2(\phi-\phi_b)\,. \tag{13b}$$

These equations were checked by numerical integrations similar to those reported by Blitz & Spergel (1991). We followed 10^4 orbits in an axisymmetric ($\psi = 0$) potential of the form (1), with starting positions and velocities distributed at random so as to give the surface density and (Gaussian) radial velocity distribution specified by equation (11). All orbits were started with $v_\phi = v_c$. Each orbit was then followed for a randomly chosen interval, to randomize its epicycle phase. Finally the perturbation amplitude was smoothly increased to ψ over 10 orbital periods, after which the stars' positions and velocities were recorded at equally spaced time intervals over a further 30 orbits. The stars were then binned in R and ϕ, and the mean velocities and velocity dispersions in each bin calculated. The predictions of equations (5a), (5b) and (13a), (13b) agreed with the simulations to within 10% as long as the vertex deviation remained smaller than about 30°.

The theoretical results in this section form the basis for the observational search for axisymmetric distortions in our Galaxy. The search employs two broad categories of test, based on the kinematics of the solar neighborhood (§ 3), and mapping of the large-scale velocity field of the Galaxy (§ 4).

2.1. *The Standard Model*

To reduce the number of free parameters, we will mainly focus on a "standard" model in which $\alpha = p = 0$, so the rotation curve is flat [$v_{\rm circ}(R) = v_{\rm circ}(R_0) = v_c$] and the equipotentials have ellipticity independent of radius (models with other rotation curves and perturbing potentials will be discussed in § 6). The standard model is somewhat unrealistic, in that normally the ellipticity would be expected to increase or decrease with radius (if the nonaxisymmetry were due to a dark halo or triaxial bulge, respectively), but it offers a simple approach to estimating the qualitative effect of nonaxisymmetry on the observations.

The nonaxisymmetric potential is specified by ϵ_Ψ (now independent of radius) and ϕ_b, or, equivalently, by the dimensionless constants

$$c_\Psi = \epsilon_\Psi \cos 2\phi_b\,, \quad s_\Psi = \epsilon_\Psi \sin 2\phi_b\,. \tag{14}$$

These parameters have at least two advantages over ϵ_Ψ and ϕ_b: (1) the perturbing potential and the dynamical response are linear in c_Ψ and s_Ψ in the limit $\epsilon_\Psi \to 0$, whereas ϕ_b is undefined when $\epsilon_\Psi \to 0$; (2) their observational consequences are generally independent—for example, a nonzero s_Ψ induces asymmetries between positive and negative longitudes, which c_Ψ does not.

For the standard model, equations (5), (9), and (13) simplify to

$$\frac{\bar v_R(\phi)}{v_c} = s_\Psi \cos 2\phi - c_\Psi \sin 2\phi\,,$$

$$\frac{\bar v_\phi(\phi)}{v_c} = 1 - c_\Psi \cos 2\phi - s_\Psi \sin 2\phi\,,$$

$$A = \frac{v_c}{2R_0}(1+c_\Psi)\,, \quad B = -\frac{v_c}{2R_0}(1+c_\Psi)\,, \tag{15}$$

$$C = \frac{v_c}{2R_0}s_\Psi\,, \quad K = -\frac{v_c}{2R_0}s_\Psi\,,$$

$$l_v = -2s_\Psi\,, \quad \delta X^2/X_0^2 = -3c_\Psi\,,$$

where all of the quantities except the velocity field are evaluated at the solar position, $R = R_0$, $\phi = 0$. Note that the streamlines have the same axis ratio as the equipotentials, but are oriented at right angles to them.

Most of the observational data that we discuss are based on line-of-sight velocities, and hence in the axisymmetric case an arbitrary uniform angular velocity can be added to the rotation curve without affecting the results (i.e., the flat rotation curve can be generalized to an arbitrary linear rotation curve). This is no longer true in the nonaxisymmetric case, since equations (15) are no longer valid if the rotation curve is not flat.

3. LOCAL CONSTRAINTS ON ELLIPTICITY

A discussion of the observational properties of the Galaxy that are sensitive to nonaxisymmetry is given by KT, and usually we simply quote their results in the section below. The error bars associated with these results are derived by the following procedure, which is somewhat arbitrary but fairly realistic. We assume that each measurement in the literature is subject to uncertainties given by (1) the error bars quoted in the original paper, plus (2) a random error that affects all measurements and that is not included in the quoted error, whose variance is determined from the spread of the values in the literature. We combine the two errors to find the weighted mean of all the measurements in the literature and its standard

[1] The condition $\sigma_{RR} \ll v_c^2$ basically means that the epicycle size is $\ll R$; however, eq. (10) is only valid if the epicycle size is also much less than the scale length for changes in the density or velocity dispersion, which is a more stringent condition.

deviation, then arbitrarily double the standard deviation to obtain an error estimate that we call the "likely" error.

3.1. *The Oort Constants*

A compilation of measurements of C and K in the literature yields the best estimates and likely errors (KT, eq. [14])

$$C = 0.6 \pm 1.1 \text{ km s}^{-1} \text{ kpc}^{-1} ; \quad K = -0.35 \pm 0.5 \text{ km s}^{-1} \text{ kpc}^{-1} , \tag{16}$$

showing no evidence for nonaxisymmetry: C and K are less than 10% of $|A|$ and $|B|$. Also note that $C + K = \bar{v}_{R,R}$, which is known to be zero within tight limits (<1 km s^{-1} kpc^{-1}) from the mean velocity and width of the H I absorption feature toward the Galactic center (Radhakrishnan & Sarma 1980; KT). In the standard model, these results imply $s_\Psi = 0.05 \pm 0.09$ from C and $s_\Psi = 0.03 \pm 0.04$ from K (using eq. [15], $v_c \approx 200$ km s^{-1}, $R_0 \approx 8$ kpc).

A recent review of measurements of A and B (Kerr & Lynden-Bell 1986) yields

$$A = 14.4 \pm 1.2 \text{ km s}^{-1} \text{ kpc}^{-1} , \quad B = -12.0 \pm 2.8 \text{ km s}^{-1} \text{ kpc}^{-1} , \tag{17}$$

where the errors are those assigned by Kerr and Lynden-Bell. In the standard model (eq. [15]), $A = -B$ whatever the nonaxisymmetric perturbation strength may be, and the observations are consistent with this result within the errors. If differences between A and $-B$ are detected, they may reflect either a nonflat rotation curve ($\alpha \neq 0$) or a radial gradient in the ellipticity ($p \neq 0$).

3.2. *Radial Motion of the Local Standard of Rest*

If the Galaxy is stationary and axisymmetric, the radial velocity $\bar{v}_R$ of the LSR should be zero. We gathered a variety of measurements of the LSR velocity relative to populations that are either near the Galactic center or representative of the Galaxy as a whole (OH/IR stars, globular clusters, high-velocity stars, planetary nebulae, etc.). We did not include CO observations, since the CO distribution in the central several hundred parsecs is asymmetric (most of the gas is at positive longitude), so that effects of Galactic rotation on the mean velocity are uncertain. (The raw average of the CO data implies that the LSR recedes from the Galactic center at ~ 14 km s^{-1}.) The combined result of these measurements (KT, eq. [15]),

$$\bar{v}_R = -1 \pm 9 \text{ km s}^{-1} , \tag{18}$$

shows no evidence for nonaxisymmetry. For the standard model, this result implies (eq. [15]) $s_\Psi = -0.01 \pm 0.05$.

3.3. *Vertex Deviation*

Young, low-dispersion populations of stars can exhibit vertex deviation as a result of spiral structure, or of incomplete mixing around their orbits since their formation; in order to use the vertex deviation to study the large-scale shape of the potential, it is therefore necessary to restrict the sample to kinematically hotter stars. Available data for populations with $\sigma_{RR}^{1/2} > 30$ km s^{-1} give (KT, eq. [26])

$$l_v = 5.5 \pm 4.2 . \tag{19}$$

Here, too, there is little or no evidence for nonaxisymmetry. For the standard model this result implies (eq. [15]) $s_\Psi = -0.05 \pm 0.04$.

3.4. *The Axis Ratio of the Velocity Ellipsoid*

In a low-dispersion axisymmetric disk, the squared axis ratio $X^2 = \sigma_{\phi\phi}/\sigma_{RR}$ is related to the local circular speed and its slope (eq. [10]), but in the solar neighborhood higher order corrections to this relation tend to increase this ratio by at least 20%–40% over the value of 0.5 appropriate for a flat rotation curve, to 0.66 ± 0.06 (eq. [12]). On the other hand, observations yield the significantly smaller value $X^2 = 0.42 \pm 0.06$ (Kerr & Lynden-Bell 1986; see also Lacey 1991, his Figs. 3 and 4). Thus

$$\frac{\delta X^2}{X_0^2} = -0.36 \pm 0.11 . \tag{20}$$

In the standard model (eq. [15]) this result implies $c_\Psi = 0.12 \pm 0.04$.

3.5. *Summary of Local Constraints*

The observations of C, K, $\bar{v}_R$, and l_v all constrain s_Ψ in the standard model, and yield an unweighted mean and standard deviation

$$s_\Psi = 0.01 \pm 0.04 . \tag{21}$$

The only local observable that constrains c_Ψ is the axis ratio X, which yields

$$c_\Psi = 0.12 \pm 0.04 . \tag{22}$$

If the standard model is correct, these results imply that $\phi_b \simeq 0$ (more accurately, $3° \pm 9°$), so the Sun lies near the minor axis of a potential with axis ratio $q_\Psi = 1 - \epsilon_\Psi = 0.88 \pm 0.04$.

The derived axis ratio is sensitive both to the assumed rotation curve and to the assumed shape of the nonaxisymmetric potential, as specified by the parameters α and p, which are both zero in the standard model. Models in which these parameters take other values are discussed in § 6.

4. LARGE-SCALE ASYMMETRY

If the Sun lies close to the symmetry axis of an elliptical potential, it is natural to ask whether the ellipticity could be detectable in the kinematics of populations that are visible at large distances from the Sun. Just as was the case for local observations, it is hard to detect, let alone measure, any distortion of the disk with even symmetry. In particular, if we are exactly on the symmetry axis, the kinematics at longitudes l and $-l$ will be the same.

Before discussing the evidence from distant objects for a distortion with even symmetry, we briefly review the evidence for odd distortions:

1. The stars at distances up to $1.5R_0$ from the Sun, in the direction of the Galactic anticenter, systematically show a mean outward motion with respect to the LSR of about 7 km s^{-1} (Lewis & Freeman 1989; Metzger & Schechter 1993), which appears to be independent of distance down the line of sight. There are at least two possible explanations for this observation: (1) the LSR is perturbed (an LSR velocity of 7 km s^{-1} is within the errors determined in § 3.2) by a local distortion with odd symmetry (similar perturbations affecting stars at other radii would tend to be washed out by limited statistics

and distance errors); or (2) there is a global perturbation with odd symmetry that gives rise to an outward motion whose magnitude changes fairly sharply near the solar radius.

2. The H I density shows systematic differences between positive and negative longitudes, which Blitz & Spergel (1991, see their Fig. 4) interpret as evidence for an elliptical distortion with odd symmetry. It is difficult to analyze this asymmetry quantitatively, since the signal is dominated by gas that lies not too far outside the solar circle;[2] however, an approximate subtraction of the local emission (Blitz 1992) does not remove the effect.

Thus there are some observations of distant objects suggesting an odd distortion is present, but the interpretation of these observations is still unclear. In any case, as noted above, the observational consequences of distortions with even and odd symmetry are usually independent as long as the perturbations are in the linear regime, and therefore the conclusions we will draw below about even distortions are independent of the nature and existence of a possible odd distortion.

For the sake of simplicity we shall first consider only the standard model, that is, a potential of the form (1) with $\alpha = p = 0$ (see § 6 for more general models). Moreover, we shall set $s_\Psi = 0$ in order to focus on the possible effects of an even distortion, described by a c_Ψ term (and from now on, when we refer to the "standard model," we shall take it to include the choice $s_\Psi = 0$).

Therefore, still working to first order in c_Ψ, and assuming $s_\Psi = 0$, we have from equations (15)

$$\bar{v}_R = -c_\Psi v_c \sin 2\phi\,, \quad \bar{v}_\phi = v_c - c_\Psi v_c \cos 2\phi\,, \tag{23}$$

both independent of radius. We can then calculate the mean line-of-sight velocity relative to the LSR for material at radius R, azimuth ϕ, observed at Galactic longitude l:

$$\bar{v}_{\rm los} = \bar{v}_\phi(R,\phi)\sin(\phi + l) - \bar{v}_\phi(R_0, 0)\sin l - \bar{v}_R(R,\phi)\cos(\phi + l) + \bar{v}_R(R_0, 0)\cos l \tag{24a}$$

$$= v_c[\sin(\phi + l) - \sin l] + c_\Psi v_c[\sin l + \sin(\phi - l)] \tag{24b}$$

$$= v_c\left(\frac{R_0}{R} - 1\right)\sin l + c_\Psi v_c[\sin l + \sin(\phi - l)]\,. \tag{24c}$$

The first line of this equation is valid for an arbitrary velocity field, but the second and third lines hold only in the standard model.

4.1. *The Distance to the Galactic Center*

If the Galaxy is axisymmetric, all objects on the solar circle $R = R_0$ should have zero line-of-sight velocity with respect to the LSR. Thus, in principle, we can search for nonaxisymmetric distortion by comparing the distances to objects with zero relative velocity to the distance to the Galactic center.

Setting $v_{\rm los} = 0$ in equation (24b), we find that the corresponding distance is

$$d = 2R_0 \cos l(1 + 2c_\Psi) + O(c_\Psi^2)\,. \tag{25}$$

This formula has been used by several authors to determine the distance to the Galactic center by assuming the Galaxy is axisymmetric, in which case $R_0 = \frac{1}{2}d/\cos l$. Here we assume instead that R_0 is known from other methods, and use the formula to constrain c_Ψ. We find

$$\frac{\text{apparent } R_0}{\text{true } R_0} = 1 + 2c_\Psi + O(c_\Psi^2)\,, \tag{26}$$

where the "apparent" R_0 is the distance to the Galactic center that would be deduced by assuming axisymmetry. If c_Ψ is as large as 0.1, the fractional error in the apparent value of R_0 determined from equation (25) is 0.2. In fact the error is even larger: equations (26) and (24) are only valid to linear order in c_Ψ, whereas a numerical solution of equation (24a) with the true velocity field of the standard model shows that the actual fractional error at $l = 45°$ is 0.25 when $c_\Psi = 0.1$ (see Fig. 1). Of course, these results only hold for the standard model ($\alpha = p = 0$). For the more general case in which the rotation curve is flat ($\alpha = 0$), but the parameter p that describes the radial dependence of the nonaxisymmetric potential (eq. [3]) is nonzero, the fractional distance error is $2c_\Psi\,(1 + \frac{1}{2}p\cos^2 l) + O(c_\Psi^2)$.

The appeal of this method is conceptual simplicity rather than robustness. In practice it is sensitive to local streaming (e.g., from spiral arms) and hence is probably not the best way to determine either R_0 or c_Ψ. The quality of the available constraints is illustrated by a recent measurement of the distance to the H_2O masers in W49(N), which lies at $l = 43°$ and has near zero line-of-sight velocity with respect to the LSR. Gwinn et al. (1989) determined the distance to W49(N), and deduced $R_0 = 7.6 \pm 1.6$ kpc assuming an axisymmetric velocity field. Their value is 1.01 ± 0.24 times the best estimate from direct methods, $R_0 = 7.5 \pm 0.9$ (obtained from the data listed by Reid 1989 that do not rely on kinematic models of the Galaxy). Taken at face value, this result implies that $-0.14 < c_\Psi < 0.10$ in the standard model, but measurements at several longitudes would be needed before a determination of c_Ψ from this method could be considered reliable.

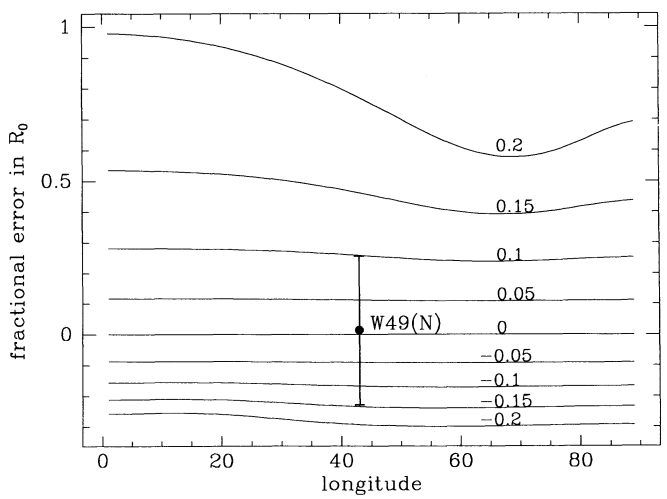

FIG. 1.—Fractional error in measurements of R_0 that are based on the distance to objects with zero line-of-sight velocity, as a function of ellipticity and Galactic longitude (§ 4.1). The Galaxy is assumed to obey the standard model (§ 2.1), the Sun is assumed to lie on a symmetry axis ($s_\Psi = 0$), and the curves are labeled by c_Ψ. The data point shows the ratio between determinations of R_0 using the distance to the maser source W49(N) (Gwinn et al. 1989) and from nonkinematic direct measurements (Reid 1989).

[2] In Blitz and Spergel's analysis the H I flux is averaged over a fixed range in Galactic latitude. The distant gas layer is thinner in projection than the latitude window used, effectively weighting against the distant emission.

4.2. *Tangent Point Measurements of the Inner Rotation Curve*

The rotation curve inside the solar circle is measured from the velocities at the tangent points, where a line of sight with $|l| < 90°$ runs tangent to a circle of constant $R < R_0$, so that the circular velocity is parallel to the line of sight. Points closer to or further from us than the tangent point lose some of their velocity in projection, and thus in an axisymmetric disk, for most realistic rotation curves, the emission from the tangent point has the highest $|v_{los}|$ of any gas along the line of sight. For conciseness, results in this subsection will be given for $0° < l < 90°$ only; the corresponding results in $-90° < l < 0°$ follow from the obvious symmetries.

We take equation (24b) at fixed longitude l, and evaluate the aximuth ϕ_m at which $(dv_{los}/d\phi) = 0$. We find

$$v_c \cos(l + \phi_m) + c_\Psi v_c \cos(\phi_m - l) = 0 , \quad (27)$$

which can be reduced to

$$\phi_m = \tfrac{1}{2}\pi - l + c_\Psi \sin 2l + O(c_\Psi^2) . \quad (28)$$

Hence to $O(c_\Psi)$ the maximum line-of-sight velocity is

$$v_m = v_c[1 - \sin l + c_\Psi(\sin l + \cos 2l)]$$
$$= v_c[1 - \sin l + 3c_\Psi(1 - \sin l) - 2c_\Psi(1 - \sin l)^2] . \quad (29)$$

If the Galaxy is axisymmetric and the rotation curve is flat, the slope of a linear fit of v_m versus $(1 - \sin l)$ is just v_c; thus from the tangent point data near $l = 90°$ we find that

$$\frac{\text{apparent } v_c}{\text{true } v_c} = 1 + 3c_\Psi . \quad (30)$$

A fit of the form $v_m \propto (1 - \sin l)$ over a larger span in l will return a slope somewhat nearer the true value of v_c; in particular, a least-squares fit between $\sin l = 1$ and $\sin l_0$ yields

$$\frac{\text{apparent } v_c}{\text{true } v_c} = 1 + \frac{3}{2} c_\Psi(1 + \sin l_0) . \quad (31)$$

Estimates of the apparent circular speed from the tangent points include 220 km s^{-1} (Gunn, Knapp, & Tremaine 1979) and 214 km s^{-1} (Rohlfs et al. 1986) from fitting between $\sin l = 1$ and $\sin l_0 = 0.5$; or 284 km s^{-1} (Rohlfs et al. 1986) and 260 km s^{-1} (Merrifield 1992) from fitting between $\sin l = 1$ and $\sin l_0 = 0.8$. Taking the means of these results, we have to $O(c_\Psi)$

$$\text{true } v_c = 272 \text{ km s}^{-1}(1 - 2.7c_\Psi) \quad \text{for} \quad \sin l_0 = 0.8 ,$$
$$\text{true } v_c = 217 \text{ km s}^{-1}(1 - 2.25c_\Psi) \quad \text{for} \quad \sin l_0 = 0.5 . \quad (32)$$

4.3. *Surveys with Absolute Distance Information*

The outer rotation curve is usually measured from velocities of tracers with known distances, such as Cepheids (Caldwell & Coulson 1989) or OB stars in H II regions (Fich, Blitz, & Stark 1989). Thus we assume that the distance to the object d, the line-of-sight velocity relative to the LSR v_{los}, and the distance to the Galactic center R_0 are known.[3] We also assume that the Galaxy is described by the standard model. Then from equation (24c) we have

$$\frac{\text{apparent } v_c}{\text{true } v_c} = 1 + c_\Psi \frac{1 + \sin\phi \cot l - \cos\phi}{R_0/R - 1} . \quad (33)$$

[3] More precisely, we require the ratios d/R_0 of the tracers to be known.

We have contoured this ratio in Figure 2 for $c_\Psi = 0.1$, as a function of position in the Galactic plane. The plot has several significant features:

1. There is a singularity at the solar circle, $R = R_0$ where the error diverges. This is the case discussed in § 4.1: when $R = R_0$ the velocity relative to the LSR is zero if the disk is axisymmetric, so no change in the rotation curve can reproduce the relative velocity caused by nonaxisymmetries.
2. Toward $l = 90°$, the ratio (apparent v_c/true v_c) is constant at $1 - c_\Psi$.
3. Near the solar position, the contours bunch together about the singularity on the solar circle. This bunching occurs because in the limit $d \ll R_0$ the line-of-sight velocity field is determined by the Oort constant A (eq. [6]), with (apparent A/true A) $= 1 + c_\Psi$ (eq. [15]).
4. In the second or third quadrants ($90° < l < 270°$), the apparent value of v_c is relatively independent of distance down the line of sight, and the fractional error is less than c_Ψ in absolute value. In the first or fourth quadrant ($0° < l < 90°$ or $270° < l < 360°$), the error is much larger, and has the same sign as c_Ψ for $R < R_0$ and the opposite sign for $R > R_0$.
5. For $R \gg R_0$,

$$\frac{\text{apparent } v_c}{\text{true } v_c} = 1 - c_\Psi(1 + 2\cos l) . \quad (34)$$

Thus in the standard model distant objects near $l = 120°$ would yield the correct value for v_c, irrespective of c_Ψ.

Most surveys of the outer Galaxy rotation curve concentrate on objects in the second and third quadrants, since they are closer: an object at $2R_0$ is 2.2 times further away at $l = 45°$ than at $l = 135°$. As shown in Figure 2, objects in these quad-

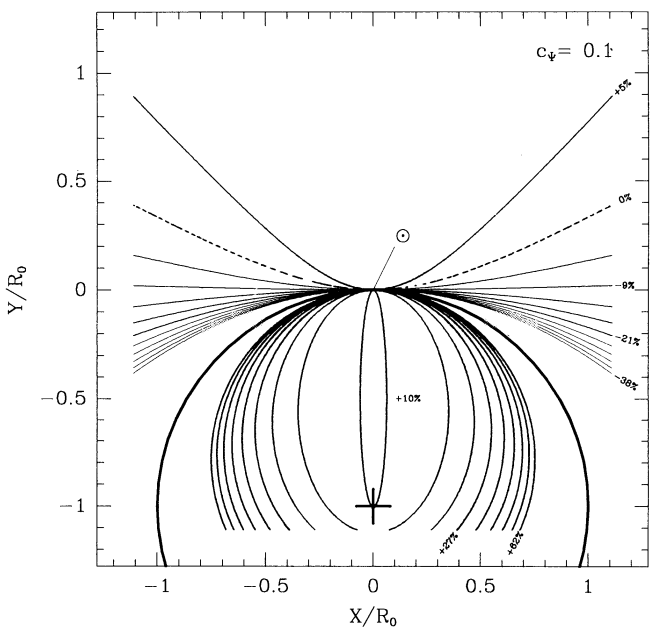

FIG. 2.—Contours showing the fractional error in the determination of the circular speed from measurement of line-of-sight velocities of tracers with known distance. The Galaxy is assumed to be of the standard model form (§ 2.1) with $s_\Psi = 0$ and $c_\Psi = 0.1$. The Sun is at $X = Y = 0$. On adjacent contours the derived circular speed differs by a factor of 1.05; the full range is a factor of 2.63 (of course, the linear approximation we have used is no longer accurate at the larger errors). On the dashed contour the error is zero; on the other contours the derived circular speed increases with contour thickness. The heavy circle centered on the cross is the solar circle, where the error diverges.

rants generally lead to an error in v_c of the same sign as c_Ψ (except close to $l = 90°$ or 270°). In sufficiently deep surveys, a comparison of distances and velocities of objects with $R > R_0$ in the first and second (or fourth and third) quadrants could be a powerful probe for nonaxisymmetric distortions, because the errors in v_c in the two quadrants would have different magnitudes and signs.

A difficulty with this approach is that absolute distances d/R_0 are much harder to measure than the relative distance d_2/d_1 of two tracers of the same type, since d and R_0 are usually determined by different methods. In practice, current measurements of the distance to the Galactic center are uncertain by about $\pm 15\%$ (§ 4.1). Figure 3 shows the devastating effect of this uncertainty. It is similar to Figure 2, but shows the ratio (apparent v_c/true v_c) arising from a 10% error in R_0 in an axisymmetric Galaxy (i.e., the distance to the Galactic center is assumed to be $0.9R_0$). The general shape of these contours is similar to those in Figure 2, suggesting that it is difficult to disentangle the effects of ellipticity from those of errors in R_0 in velocity surveys. This problem will be investigated in more detail in § 4.4.

The H II-region survey of Fich et al. (1989) is an example of a modern survey with "absolute" distances. They analyzed their data with the standard IAU values $R_0 = 8.5$ kpc and $v_c = 220$ km s^{-1}, which resulted in a flat rotation curve. They also repeated the analysis with different values for R_0, and found equally acceptable rotation curves for a wide range from 5 to 10 kpc, $R_0 = 6$ kpc giving the best fit to a power-law rotation curve. There is a 25% uncertainty in the distance scale for the stars embedded in the H II-regions, large enough that there is little hope of separating the effects of distance errors from the signal of any plausible "even" ellipticity of the disk.

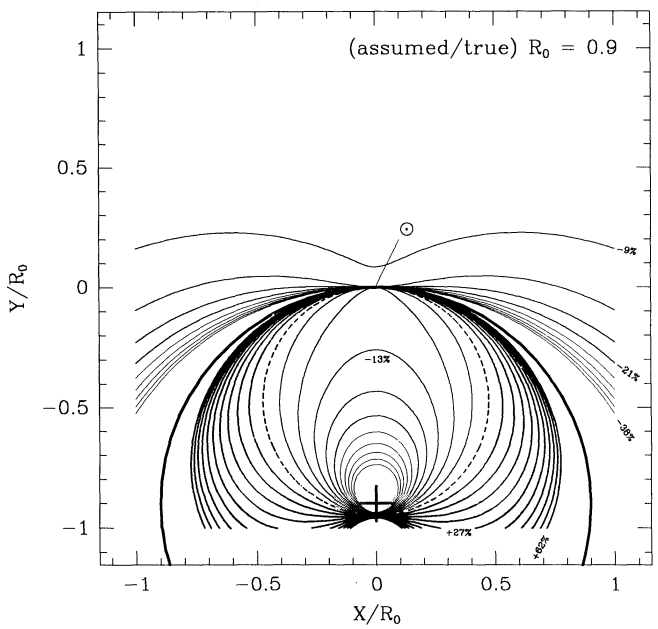

FIG. 3.—Same as Fig. 2, except that the Galaxy is assumed to be axisymmetric and the distance to the Galactic center is mistakenly taken to be $0.9R_0$. The heavy circle shows the solar circle calculated with the erroneous distance to the Galactic center, and the cross the corresponding location of the Galactic center. Note the similarity of the pattern of deviation to Fig. 2, particularly outside the solar circle, which implies that it is difficult to distinguish the effects of an error in R_0 from ellipticity of the Galactic disk.

4.4. *Surveys with Relative Distance Information*

An alternative approach, which does not require measuring absolute distances, is to tie the distance scale to R_0 from the observations themselves, essentially by measuring the curvature of the velocity field over distances $\sim R_0$ or greater. This approach is described by Schechter et al. (1989) for their carbon-star data. We will follow their analysis technique, which involves a least-squares fit of all the data to a flat rotation curve, varying the parameters R_0 and v_c to obtain the best fit to the data.

To illustrate how this approach can work in principle, we consider the case of tracers at large distances, $d \gg R_0$: in this limit, to $O(R_0/d)$ we have $R_0/R = R_0/d$, $\sin\phi = \sin l + (R_0/d)\sin l \cos l$ and $\cos\phi = -\cos l + (R_0/d)\sin^2 l$, so that equation (24c) becomes

$$v_{\rm los} = v_c\left(\frac{R_0}{d} - 1\right)\sin l + c_\Psi v_c \sin l\left(1 + 2\cos l + \frac{R_0}{d}\cos 2l\right) + O\left(\frac{R_0}{d}\right)^2 . \quad (35)$$

Fitting the slope and intercept of this linearized function of d^{-1} to the analogous expression for a circular disk, we have to $O(c_\Psi)$,

$$\frac{\text{apparent } v_c}{\text{true } v_c} = 1 - c_\Psi(1 + 2\cos l)\,,$$

$$\frac{\text{apparent } R_0}{\text{true } R_0} = 1 + 2c_\Psi(\cos^2 l + \cos l)\,; \quad (36)$$

the first of these expressions is the same as equation (34). Thus, for very deep surveys, data at a single longitude suffice in principle to provide apparent values for R_0 and v_c, which however vary with longitude if the disk is not axisymmetric. At present, the determination of R_0 and v_c from observations at a single longitude is not practical: the reason is that maximum tracer distances are only $d \approx R_0$, so that determining the asymptotic value of $v_{\rm los}$ as $R_0/d \to 0$ requires a large extrapolation. There is of course also no guarantee that the rotation curve remains flat at very large radii.

The freedom to vary R_0 is a very great one in fits to data with $d \lesssim R_0$, as can be seen from the similarity of the error contours in Figures 2 and 3. In the limit $d \ll R_0$, line-of-sight velocity data can only constrain the Oort constant $A = \frac{1}{2}$ [apparent (v_c/R_0)], so best-fit values for v_c and R_0 from such data will be highly correlated.

To illustrate what can be learned from the data, we carried out several simulations. In our first simulation, we mimicked a deep survey near the direction of Galactic rotation, by sampling 50 stars uniformly spread along each of the lines of sight $l = 50°$, 70°, 90°, 110°, and 130° out to distances of R_0 from the Sun. We determined their line-of-sight velocities in the standard model from equation (24c). Each stellar velocity was assumed to have an additional random Gaussian scatter of dispersion $\sigma_v = 0.1v_c$, due to velocity dispersion and measurement errors. We then used least-squares fitting to determine the best apparent values of v_c and R_0 for an axisymmetric model Galaxy with a flat rotation curve.

For c_Ψ between -0.2 and 0.2, the best-fit parameters are tabulated in Table 1. The last column shows $\sigma_{\rm fit}$, defined so that the mean-square deviation between the best-fit model and the observed velocities is $\sigma_v^2 + \sigma_{\rm fit}^2$; thus $\sigma_{\rm fit}$ is the standard

TABLE 1

ERRORS IN v_c AND R_0 DETERMINED FROM A VELOCITY SURVEY WITH KNOWN RELATIVE DISTANCES IN AN ELLIPTICAL DISK

c_Ψ	apparent v_c / true v_c	apparent R_0 / true R_0	Covariance	σ_{fit} / true v_c
−0.20.....	0.694 ± 0.036	0.676 ± 0.029	66%	0.0159
−0.15.....	0.755 ± 0.038	0.747 ± 0.031	64%	0.0118
−0.10.....	0.825 ± 0.040	0.824 ± 0.034	63%	0.0079
−0.05.....	0.906 ± 0.044	0.907 ± 0.038	64%	0.0040
0.00.....	1.000 ± 0.048	1.000 ± 0.044	66%	0.0000
0.05.....	1.112 ± 0.054	1.105 ± 0.051	69%	0.0040
0.10.....	1.246 ± 0.064	1.226 ± 0.064	75%	0.0080
0.15.....	1.411 ± 0.077	1.368 ± 0.079	81%	0.0121
0.20.....	1.617 ± 0.099	1.536 ± 0.100	86%	0.0163

NOTES.—Second and third columns contain the ratio between best-fit and true values for the circular speed v_c and distance to the Galactic center R_0, as determined from a survey of line-of-sight velocities containing 50 stars in each of the five directions $l = 50°$, 70°, 90°, 110°, and 130°. The stars are uniformly distributed in distance out to R_0. The Galaxy is described by the standard model (eq. [24c]), with ellipticity measured by c_Ψ. Each stellar velocity has a random scatter with standard deviation $\sigma_v = 0.1v_c$. The covariance is between the measured values of v_c and R_0, and $\sigma_{fit}^2 + \sigma_v^2$ is the mean-square deviation between the best-fit model and the velocities.

deviation of the distribution of residual velocities in the limit $\sigma_v \to 0$. Figure 4 shows contours of constant χ^2 for each of the lines of sight individually as well as for the total sample of all five lines of sight, in the particular case $c_\Psi = 0.1$. It shows that data with $90° < l < 270°$ hardly place independent constraints on v_c and R_0, whereas data with $|l| < 90°$ do: the combined data set therefore yields a decent constraint on each parameter, albeit with some correlation between the best-fit values obtained. The χ^2 contours in Figure 4, when projected onto the coordinate axes, correspond to n-σ deviations from the best fit, for $n = 1$ to 5; the derived error bounds of around 5% on v_c and R_0 will scale with the velocity scatter σ_v and number of stars observed N as $\sigma_v N^{-1/2}$, provided $\sigma_v \gg \sigma_{fit}$.

Not surprisingly, the fitted R_0 is very close to the value required to force zero line-of-sight velocity on the solar circle (eq. [26]): this is because the inner Galaxy lines of sight provide the best constraints on R_0, while the remaining data only really determine a single combination of R_0 and v_0. When the error $\sigma_v \to 0$, the rms scatter of these simulated data about the best axisymmetric, flat rotation curve fit is approximately given by $0.08|c_\Psi|v_c$. Even for c_Ψ as large as 0.2, this rms scatter of $\sim$4 km s^{-1} would be well buried in the scatter from measurement errors and the velocity dispersion of the tracers; thus it would be very hard to detect nonaxisymmetry from such a survey. Figure 5 shows the residuals of the data about the best fit, for $c_\Psi = 0.1$ and several different longitudes.

Next we simulated a survey with the same number of stars per line of sight, more complete sky coverage ($30° < l < 150°$) but less depth ($d < \frac{1}{2}R_0$). The best-fit parameters are given in Table 2. Even though the total number of stars is larger, the errors on v_c and R_0 are much larger than in Table 1: the velocities are now smaller, and so more stars are needed to obtain the same signal above the velocity dispersion "noise." The fitted value for R_0 is now closer to the true one; it deviates more from the value required to force zero line-of-sight veloc-

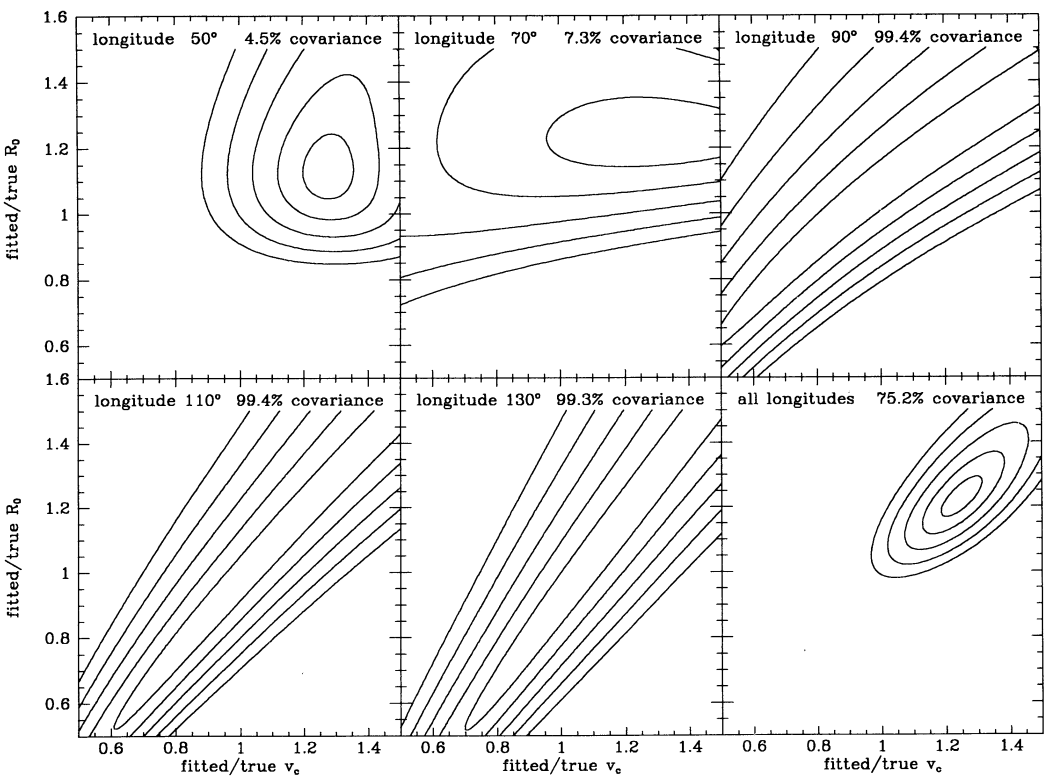

FIG. 4.—Contours of constant χ^2 (goodness of fit), for tracers with known line-of-sight velocity and relative distance (cf. Table 1). The tracers are drawn from a standard model with $s_\Psi = 0$, $c_\Psi = 0.1$, and fitted by an axisymmetric model having a flat rotation curve with adjustable circular speed v_c and distance to the Galactic center R_0. The sample consists of 50 stars at distances up to R_0, with rms velocity errors of $0.1v_c$, from each of five lines of sight uniformly spaced between $l = 50°$ and $l = 130°$. The first five panels show the constraints placed by the individual lines of sight; the final panel applies to the entire data set. Covariances between the fit parameters are indicated. Contours of 1, ..., 5 σ deviations from the best fit are shown.

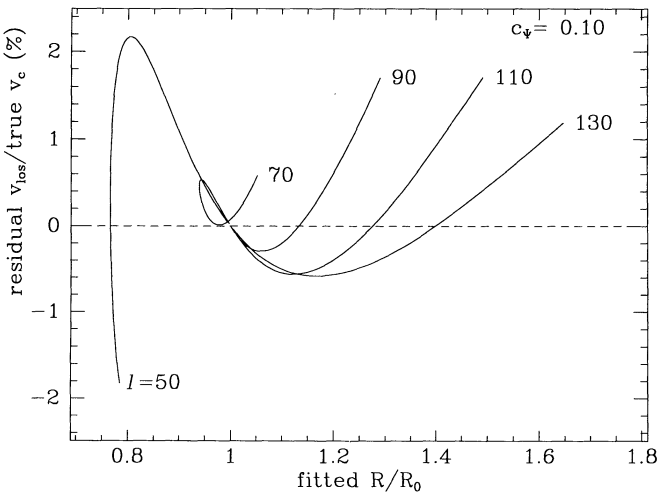

FIG. 5.—rms residuals of line-of sight velocities in the model of Fig. 4 and Table 1, relative to the best-fit axisymmetric, flat rotation curve model with adjustable v_c and R_0. Note the small amplitude of the residuals (given as multiples of the true v_c), which implies that velocity surveys of this kind perform poorly in detecting nonaxisymmetric distortions if the Sun is near a symmetry axis.

ity on the solar circle (eq. [26]) than the deeper survey simulated above, because less of the solar circle falls within the sampling volume. The rms scatter about the best fit is $0.055|c_\Psi|v_c$, once again small enough that nonaxisymmetry would be very difficult to detect.

These simulations were chosen to be crudely similar to two recent deep velocity surveys, one of carbon stars to distances of about R_0 (Schechter et al. 1989), and the other of Cepheids to distances of about $\frac{1}{2}R_0$ from the Sun (Caldwell & Coulson 1989). These surveys yield

$$\begin{aligned} v_c &= 248 \pm 16 \text{ km s}^{-1} \quad \text{(carbon stars)}, \\ v_c &= 228 \pm 19 \text{ km s}^{-1} \quad \text{(Cepheids)}, \end{aligned} \tag{37}$$

when analyzed assuming a flat rotation curve and axisymmetry.

The carbon star survey does not yield an absolute distance calibration. The Cepheid survey does: combining their result with a calibration derived from nearby cluster Cepheids, Caldwell & Coulson (1989) derive $R_0 = 7.8 \pm 0.7$ kpc. Compared with the direct estimate of 7.5 ± 0.9 kpc (§ 4.1), we get a ratio between apparent and true R_0 of 1.04 ± 0.15. Thus we deduce from Table 2 the very weak constraint $-0.16 < c_\Psi < 0.30$. (If there were sufficient data to reduce the observational errors in Table 2 to zero, we would obtain $-0.08 < c_\Psi < 0.15$.) This illustrates once again the difficulty of separating errors in R_0 from the signal due to ellipticity.

TABLE 2

ERRORS IN v_c AND R_0 DETERMINED FROM A VELOCITY SURVEY WITH KNOWN RELATIVE DISTANCES IN AN ELLIPTICAL DISK

c_Ψ	apparent v_c / true v_c	apparent R_0 / true R_0	Covariance	σ_{fit} / true v_c
−0.20.....	0.586 ± 0.092	0.725 ± 0.115	93%	0.0104
−0.15.....	0.682 ± 0.105	0.799 ± 0.122	93%	0.0080
−0.10.....	0.782 ± 0.120	0.868 ± 0.131	94%	0.0054
−0.05.....	0.888 ± 0.137	0.935 ± 0.141	95%	0.0027
0.00.....	1.000 ± 0.154	1.000 ± 0.149	95%	0.0000
0.05.....	1.121 ± 0.171	1.067 ± 0.159	96%	0.0028
0.10.....	1.249 ± 0.199	1.133 ± 0.175	96%	0.0055
0.15.....	1.386 ± 0.218	1.200 ± 0.183	97%	0.0083
0.20.....	1.531 ± 0.240	1.268 ± 0.194	97%	0.0110

NOTES.—Same as in Table 1, but for a survey of 50 stars, out to distance $0.5R_0$, in each of the seven directions $l = 30°$, 50°, 70°, 90°, 110°, 130°, and 150°.

The sign of the effect of a c_Ψ-term on the deduced value of v_c can be understood qualitatively: radial velocity surveys basically yield the combination of parameters $v_c = 2AR_0$, and both the Oort constant A (eq. [15]) and the apparent (kinematic) distance to the Galactic center R_0 (eq. [26]) are increased by a positive c_Ψ; thus the value of v_c is affected in the same direction on both counts.

The discussion above is not intended to be an exhaustive analysis of the effects of ellipticity on velocity surveys. Nevertheless, it illustrates two important points: first, that velocity surveys of tracers with only relative distance calibration, out to distances $\lesssim R_0$, are insensitive to disk ellipticity if the Sun is near a symmetry axis; second, that modest ellipticities (say, $|c_\Psi| < 0.1$) can substantially affect determinations of the circular speed from such surveys (by up to 25%). Isolating evidence for ellipticity from velocity surveys will require either surveys with greater depth, or an independent determination of R_0 or v_c to higher accuracy than so far has been achieved.

4.5. *Merrifield's Method*

An alternative way to measure distances is to determine the distribution of a population of tracers on the sky and then estimate distance in units of R_0, using the fact that we are offset from the center of the Galaxy. The most successful application of this method so far is that of Merrifield (1992), who used the angular scale height of H I emission as a measure of distance. Earlier attempts based instead on the surface density of H I gas (Petrovskaya & Teerikorpi 1986) turned out to be sensitive to errors caused by the irregular distribution of H I clouds in the outer Galaxy.

We now summarize Merrifield's method for extracting kinematic distances from the observed H I distribution in (l, b, v_{los}). In an axisymmetric disk, equation (24a) implies that

$$v_{los} = \left[\frac{R_0}{R} v_{circ}(R) - v_c\right] \sin l \equiv W(R) \sin l , \tag{38}$$

where, as usual, $v_c = v_{circ}(R_0)$ is the circular speed at the solar radius. Provided $W(R)$ is monotonic, which is usually the case, all gas with the same observed $W = v_{los}/\sin l$ lies in a ring at a single radius R from the Galactic center. Merrifield observed that, provided $R > R_0$, the distance to such a ring can be measured by looking at the variation in its projected extent in Galactic latitude b around the sky. If the characteristic height $\Delta z(R)$ of the gas is the same at all azimuths, the projected latitude width Δb should vary in a characteristic manner with longitude:

$$\Delta b = \frac{\Delta z}{R_0 \cos l + \sqrt{R^2 - R_0^2 \sin^2 l}}, \quad R > R_0 . \tag{39}$$

By fitting this variation, the radius of each slice of constant W can be determined (in units of R_0), and used to construct the rotation curve of the outer Galaxy for assumed values of R_0 and v_c, via

$$v_{circ}(R) = \frac{R}{R_0}[W(R) + v_c] . \tag{40}$$

With this method, Merrifield (1992) obtained a rotation curve for the Galaxy out to $R \simeq 2R_0$; his results imply that the outer rotation curve is approximately linear in R (i.e., $W(R)$ is linear in R^{-1}, see his Fig. 2) and can be fit by the expression

$$v_{\rm circ}(R) = 165 \text{ km s}^{-1}\left(1 - \frac{R}{R_0}\right) + v_c \frac{R}{R_0}, \quad (41)$$

so $v_c = 165$ km s^{-1} if the rotation curve is flat. This result led him to argue that either the Galaxy has the most steeply rising rotation curve of all nearby, well-observed Sbc galaxies or v_c should be decreased from its standard (IAU) value of 220 km s^{-1} to 200 km s^{-1} or even lower.

How is this striking conclusion affected by an elliptical distortion of the disk? To provide an analytic illustration, we consider only the gas near the directions $l = 0$ and 180°. In these directions the projected latitude widths are at opposite extremes, and values of R derived from the ratio of these widths are a reasonable approximation to the result of a fit of Δb to equation (39) over all longitudes. (Note that we concentrate on gas near $l = 0°$ and 180° for the sake of mathematical simplicity only. In reality the emission from all radii has the same velocity in these directions, and hence the separation of different W = constant curves is impossible. However, the center and anticenter directions provide a first-order approximation to the projected scale heights around these longitudes; we have checked that a longitudes as much as 60° either side of the center and anticenter directions, which carry the dominant signal in Merrifield's determination of $R(W)$, a similar treatment results in the same apparent circular speed to within 5%.)

Near the Galactic anticenter (AC), $l \simeq \pi$, $\phi \simeq (1 - R_0/R)(\pi - l)$, so equation (24b) for the standard model yields

$$R \lim_{l \to \pi} \frac{v_{\rm los}}{\sin l} \equiv RW_{\rm AC} = (R_0 - R)v_c + c_\Psi(R_0 - R)v_c, \quad (42)$$

while for gas beyond the Galactic center (GC) with $l \simeq 0$, $\phi \simeq \pi - (1 + R_0/R)l$ and hence

$$RW_{\rm GC} = (R_0 - R)v_c + c_\Psi(R_0 + 3R)v_c. \quad (43)$$

Thus, gas observed near the AC or GC with a given W lies at radius

$$R_{\rm AC} = \frac{v_c(1 + c_\Psi)}{W + v_c(1 + c_\Psi)} R_0 \quad \text{or} \quad R_{\rm GC} = \frac{v_c(1 + c_\Psi)}{W + v_c(1 - 3c_\Psi)} R_0, \quad (44)$$

whence it presents a projected width

$$\Delta b_{\rm AC} = \frac{\Delta z(R_{\rm AC})}{R_{\rm AC} - R_0} \quad \text{or} \quad \Delta b_{\rm GC} = \frac{\Delta z(R_{\rm GC})}{R_{\rm GC} + R_0}. \quad (45)$$

Assuming axisymmetry would lead one to deduce a radius R_W, generally incorrect, for the constant-W ring of gas of

$$R_W = \frac{\Delta b_{\rm AC} + \Delta b_{\rm GC}}{\Delta b_{\rm AC} - \Delta b_{\rm GC}} R_0. \quad (46)$$

The assumption of axisymmetry and constant rotation speed would then lead to an apparent rotation speed given by (eq. [38])

$$\frac{\text{apparent } v_c}{\text{true } v_c} = -\frac{W}{2v_c}\left(\frac{\Delta b_{\rm AC}}{\Delta b_{\rm GC}} + 1\right). \quad (47)$$

To $O(c_\Psi)$ we then have

$$\frac{\text{apparent } v_c}{\text{true } v_c} = 1 + \frac{c_\Psi}{(1 + w)^2} \times [w^2 + 4w + 3 - 2(2 + w)R_0(\ln \Delta z)_{,R}], \quad (48)$$

where $w = W/v_c$.

Some comments on this expression are in order:

1. The expression simplifies in the limit $R \gg R_0$, where $w \to -1$, to the form

$$\frac{\text{apparent } v_c}{\text{true } v_c} = 1 + 2c_\Psi \frac{R}{R_0}[1 - (\ln \Delta z)_{,\ln R}]. \quad (49)$$

Notice that the error caused by a fixed distortion c_Ψ grows at larger radii. Also, in this limit it can be shown that the effects of a nonaxisymmetric distortion mimic the effect of a change in circular speed at all longitudes, not just toward the Galactic center and anticenter.

2. In Merrifield's (1992) analysis of the outer H I distribution, a typical value of w is -0.5 ($R = 2R_0$), which implies

$$\frac{\text{apparent } v_c}{\text{true } v_c} = 1 + c_\Psi[5 - 6(\ln \Delta z)_{,\ln R}] \quad (50a)$$

$$\simeq 1 - 1.0c_\Psi, \quad (50b)$$

where in equation (50b) we have used $(\ln \Delta z)_{,\ln R} = 1$ for the flaring rate, which is a typical value estimated by Merrifield. Note that the large numerical coefficients in the square brackets nearly cancel for the particular value of the flaring rate chosen in equation (50b); thus there is substantial uncertainty in the result (50b) (cf. the numerical simulation below).

3. An oversimplification in our derivation is that we have neglected the possibility of azimuthal variations in the scale height Δz at fixed radius. The fractional amplitude of such variations is difficult to estimate without first understanding the three-dimensional shape of the nonaxisymmetric potential, but is probably of order c_Ψ. A justification for their neglect is that near the directions $l = 0°$ and 180° the twofold symmetry of the elliptical distortion ensures that the scale heights are the same at corresponding radii; [the scale height of a self-gravitating gas layer varies in inverse proportion to the surface density, provided the velocity dispersion remains the same; in the standard model the disk scale height would vary $\propto(1 - c_\Psi \cos 2\phi)$] more generally, any twofold distortion of the actual scale height is largely decoupled from the asymmetric distortion of the apparent scale height caused by our offset from the center.

We have carried out numerical simulations of the effect of ellipticity on Merrifield's determination of the rotation curve. We assumed that the scale height of the gas along the $l = 0$, 180° axis was given by a relation of the form

$$\Delta z = \begin{cases} z_0, & \text{for } R < R_0, \\ z_0[1 + s(R/R_0 - 1)], & \text{for } R > R_0, \end{cases} \quad (51)$$

where s is a measure of the flaring of the gas layer; Merrifield finds $s \simeq 1.4$ for an axisymmetric disk. (A linear relation of the form [51] is a better description of flaring observed in disk galaxies than, for example, a power-law $\ln \Delta z_{,\ln R}$ = constant.) We then constructed "apparent" rotation curves for $-0.2 < c_\Psi < 0.2$ according to equations (42)–(47), and read off the circular speed deduced from data at $l \simeq 0$, 180° and

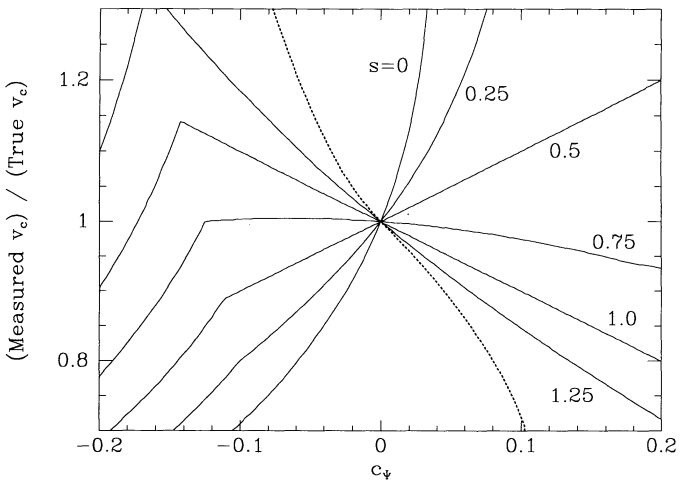

FIG. 6.—Ratio between apparent and true circular speed that would be derived with Merrifield's method in an elliptical Galaxy described by the standard model. The solid curves are labeled with the different values used for the flaring parameter s, as defined in eq. (51). The kinks are caused by the discontinuous change in the slope of the scale height vs. radius relation that occurs at R_0 in eq. (51). The dotted curve connects those models that reproduce the flaring seen in the data.

(apparent) radius $R = 2R_0$. These circular speeds are plotted as solid curves in Figure 6, for different ellipticities and flarings. The kinks at negative c_Ψ seen in these curves are caused by the abrupt change in the slope of the scale height at the solar radius, showing that the analysis with an axisymmetric model can incorrectly place gas that is really inside the solar circle at radii beyond $2R_0$, when $c_\Psi \lesssim -0.1$. Over the plotted range of positive c_Ψ, this does not happen, and moreover the derived rotation curves are linear to a good approximation.

As demonstrated in equation (50a) and Figure 6, the sign and magnitude of the change in apparent circular speed depend sensitively on the ellipticity and flaring of the outer disk. However, not all of the models considered in Figure 6 are good representations of the H I data, as they must also reproduce the apparent flaring of the gas. The dotted line in Figure 6 connects the models that have apparent $\Delta z(2R_0)/\Delta z(R_0) \simeq 2.4$ (equivalent to $s = 1.4$), as Merrifield finds from the actual H I data. For the roundest model consistent with the results derived in § 3, with $c_\Psi = 0.08$, Merrifield's analysis underestimates the true value of v_c by 20%, and the true flaring rate s would be about 1.9.

5. COMPARISONS BETWEEN THE METHODS: SIGNS OF ELLIPTICITY?

The different determinations of the circular speed v_c listed in §§ 4.2–4.5 do not agree very well, and the cause(s) of the differences between these determinations are obscure. Here we investigate the hypothesis that all measurements are affected by an elliptical distortion of the disk, and try to build a coherent picture in which they might be reconciled. We focus our attention on the standard model (§ 2.1), although a thorough investigation would require analyzing a much broader class of models (see § 6). We emphasize once again that the large-scale data we have analyzed only constrain the even perturbation terms (c_Ψ).

Each measurement of the "apparent" v_c from the nearby and far H I tangent points, the carbon star and Cepheid velocity surveys, and the outer Galaxy H I (respectively, 272 and 217 km s^{-1} from eq. [32], 248 and 228 km s^{-1} from eq. [37], and 165 km s^{-1} from eq. [41]) can be converted with our simple simulations into a relation between the "true" v_c and c_Ψ. These relations, obtained from Tables 1 and 2, equations (32), and Figure 6 are plotted in Figure 7. While the H I tangent point data and the stellar velocity surveys are all affected in more or less the same way by ellipticity, tending to overestimate the circular speed for positive c_Ψ, Merrifield's reliance on a distinct kind of distance indicator biases his result quite differently. The different relations can be reconciled if $c_\Psi \simeq 0.08$, $v_c \simeq 200$ km s^{-1} (the rms spread among methods of the deduced "true" circular speeds is 14 km s^{-1}, as compared to 40 km s^{-1} for the apparent values[4]), suggesting that ellipticity in the outer disk may be the source of much of the apparent discrepancy between the different data sets. These parameters correspond to an axis ratio for the equipotentials of 0.92, with the Sun near the minor axis. The axis ratio of the streamlines is the same in the standard model, with the long axis of the streamlines oriented at right angles to the long axis of the equipotentials.

The local constraints examined in § 3 also point towards an ellipticity near 0.1 in the context of our standard model. The shaded bands in Figure 8 represent the 1 σ regions of the (v_c, c_Ψ)-plane allowed by the observed values of the Oort constants A and B, and the velocity ellipsoid axis ratio X, using $A = 14.4 \pm 1.2$ km kpc^{-1}, $B = -12.0 \pm 2.8$ km s^{-1} kpc^{-1} and $R_0 = 7.5 \pm 0.9$ kpc (see § 3 and § 4.1). The three bands intersect near $c_\Psi = 0.12$, $v_c = 180$ km s^{-1}: a formal best-fit solution to these local data gives

$$c_\Psi = 0.12 \pm 0.04\,, \quad v_c = 181 \pm 26 \text{ km s}^{-1}\,, \quad \chi^2 = 0.4 \quad (1 \text{ d.o.f.})\,. \tag{52}$$

[4] The most discrepant curve in Fig. 7 comes from tangent point data fitted down to $R = \frac{1}{2}R_0$. This discrepancy could indicate a change of either the circular speed or the axis ratio in the inner Galaxy, where the relative contributions of the bulge, halo and disk to the rotation curve are changing rapidly with radius (e.g., Kuijken & Gilmore 1989). The other four curves, which span data over a similar radial range $0.8R_0 < R < 2.5R_0$, agree nicely.

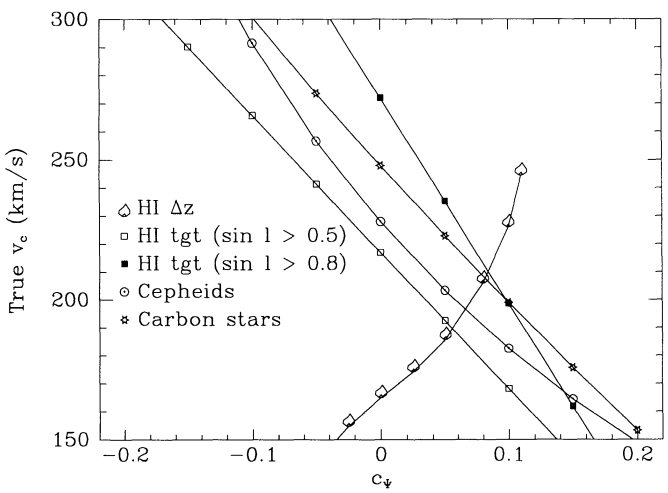

FIG. 7.—"True" circular speed derived from different data sets, corrected for different assumed ellipticities in the context of the standard model with $s_\Psi = 0$. H I Δz: Merrifield's method (§ 4), from Fig. 6; H I tgt: H I tangent points (§ 4.2), from eq. (32); Cepheids and carbon stars: from eq. (37), with corrections derived from simulated data in Tables 1 and 2. The convergence near $c_\Psi = 0.08$ of the curves for outer Galaxy data is evidence for an elliptical disk.

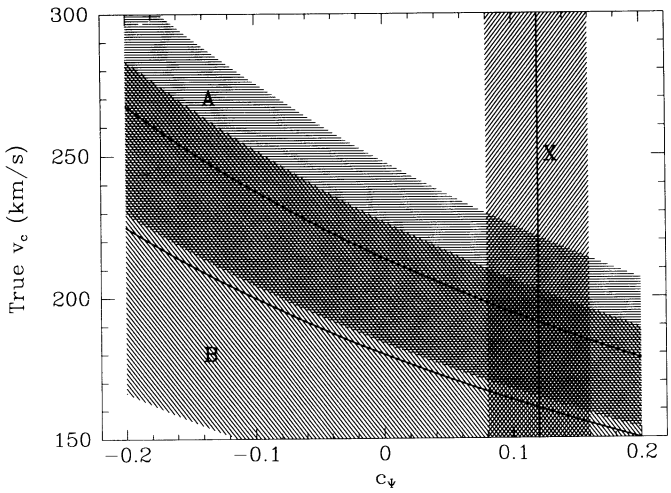

FIG. 8.—"True" circular speed derived from local observations, in the context of the standard model with $s_\Psi = 0$. Cross-hatched regions are allowed at the 1 σ level by constraints from the axis ratio of the velocity ellipsoid (X, see § 3.4) and from the Oort constants A and B (§ 3.1). As in Fig. 7, the data point toward an ellipticity near $c_\Psi = 0.1$.

Thus, local and global data *independently* point toward an ellipticity of the Galactic disk of about 0.1, with the Sun near the minor axis of the potential, and a circular speed well below the IAU standard value of 220 km s^{-1}.

6. MORE GENERAL ELLIPTICAL DISK MODELS

So far, we have concentrated our analysis on the standard model in which the rotation curve is flat and the equipotential curves have the same ellipticity at all radii ($\alpha = p = 0$ in the notation of eqs. [2] and [3]). We now relax these assumptions, allowing nonzero values for the exponents α and p. Thus the ellipticity parameter c_Ψ (eqs. [4] and [14]) is a function of radius, $c_\Psi(R) \equiv c_\Psi(\odot)(R/R_0)^{p-2\alpha}$. We continue to search for even perturbations (c_Ψ) only, and to assume that the potential is stationary.

The velocity field in these more general models was given in equations (5a) and (5b). The axis ratio of the velocity ellipsoid for "warm" stars in an axisymmetric model is assumed to be given by (cf. eqs. [10] and [12])

$$X_0^2 = 0.66 + \tfrac{1}{2}\alpha \pm 0.06 , \qquad (53)$$

where we have assumed that the velocity dispersion-dependent correction to the axis ratio is independent of α. We have confirmed that this relation is adequate with orbit integrations of the type described in the introduction to § 2.

For each choice of the four parameters v_c, $c_\Psi(\odot)$, α and p, our simulations predict the amplitude of the best-fit flat rotation curve to the tangent point data (§ 4.2), distant stars (§ 4.4), and the thickness of the H I layer (§ 4.5), as well as local quantities: the Oort constants A, B (§ 3.1), and the axis ratio X (§ 3.4). Assigning observational errors of 20 km s^{-1} to each of the measurements of v_c from distant data, and using the errors on A, B, and X given in equations (17) and (53), we can form a χ^2 statistic that tests the predictions of these four parameters against observed values. Projections of this statistic onto the various possible two-parameter planes, obtained by minimizing χ^2 over the suppressed variables, are presented in Figure 9. The best-fit model (marked by a dot in each panel) has $\chi^2 = 2.0$ (4 degrees of freedom), with parameters $v_c = 184$ km s^{-1}, $c_\Psi(\odot) = 0.08$, $\alpha = -0.1$, $p = 0.1$. The best-fit standard model (for which $\chi^2 = 3.6$, 6 degrees of freedom) has ellipticity 0.082 and circular speed 197 km s^{-1}. Both fits are quite satisfactory, with no statistically significant improvement in the goodness of fit of the four-parameter models over the standard model. Axisymmetric models appear to be ruled out quite strongly ($\chi^2 > 9$, corresponding to a likelihood that is lower than the best-fit elliptical model by 2.6 σ), with the best fits requiring, implausibly, that $\alpha \simeq -0.45$, which would give the Milky Way the most steeply falling rotation curve known among large spiral galaxies.

The χ^2-contours are rather asymmetric, showing a marked truncation for p above the best-fit value. The truncation arises because the H I layer thickness analysis of § 4.5 breaks down at a radius below $2R_0$ for quite small ellipticities when $p > 0$: at larger c_Ψ, no constant-W slice in these models will have the required ratio of 1:3 between the projected angular scale heights near $l = 0°$ and 180° if the H I layer flares as is observed. These models therefore cannot reproduce the observed data. As can be seen in Figure 9, at positive p the best-fit model tends to lie close to the maximum ellipticity for which the analysis still works, and as a result the error distribution is skewed rather strongly. Nevertheless, we can obtain approximate 1 σ confidence intervals for the four parameters from the innermost χ^2-contours:

$$v_c = 184^{+19}_{-14} \text{ km s}^{-1} , \quad c_\Psi(\odot) = 0.08^{+0.04}_{-0.03} ,$$
$$\alpha = -0.1^{+0.1}_{-0.1} , \quad p = 0.1^{+0.3}_{-0.6} . \qquad (54)$$

The analogous result for the standard model is

$$v_c = 197 \pm 9 \text{ km s}^{-1} , \quad c_\Psi = 0.082 \pm 0.014 ; \qquad (55)$$

since allowing α and p to vary produces no significant improvement in the fits we shall adopt the values (eq. [55]) throughout the rest of this paper.

In summary,

1. The standard model provides a satisfactory description of an elliptical distortion that could explain the observed peculiarities in Galactic rotation and kinematics;
2. The best-fit four parameter model in which the ellipticity and rotation curve are power-law functions of radius has a slightly falling rotation curve ($v_{\rm circ} \propto R^{-0.1}$), but the improvement in the fit over the standard model is not statistically significant;
3. Axisymmetric models give poor fits to the data.

We have not explored at least two remaining free parameters, a nonzero pattern speed or other azimuthal wavenumbers than $m = 2$.

7. ASYMMETRIES IN THE OUTERMOST GAS

It has often been noted that the H I distribution in the Galaxy is not symmetric about the axis $l = 0°$–180°. The most recent and thorough investigation of this phenomenon has been carried out by Blitz & Spergel (1991), who showed that much of the large-scale asymmetry can be explained by postulating an outward motion of the LSR of about 14 km s^{-1}. They then constructed a model in which this motion is the result of a rotating quadrupole potential with an inner Lindblad resonance near $R = 1.5R_0$ and long axis near $\phi = 135°$, and showed that their model is consistent with many observational constraints.

Subsequently, Kuijken (1991) has argued that a lopsided

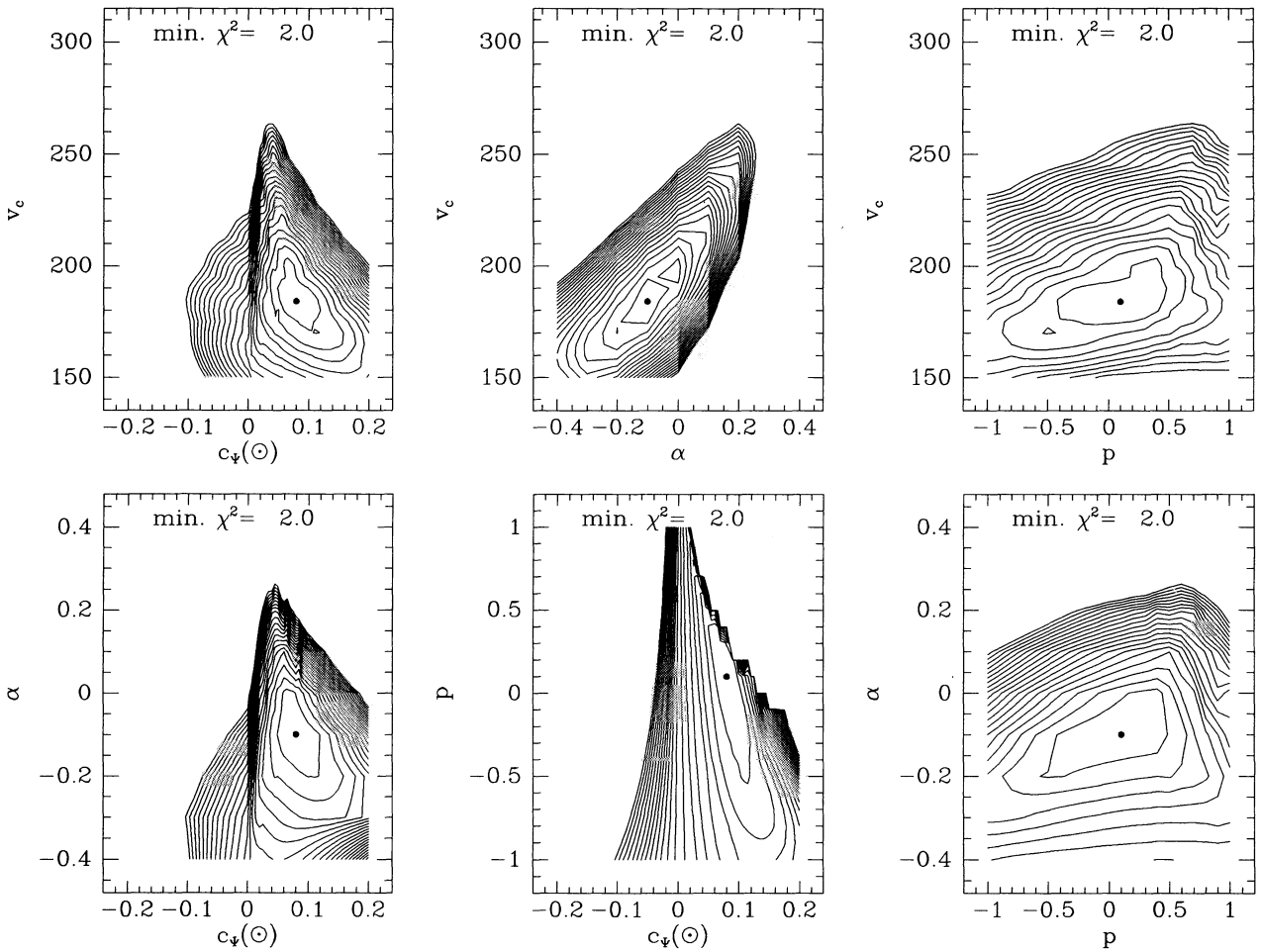

FIG. 9.—Projections of χ^2 for four-parameter model fits of local and rotation curve data to elliptical disk models. v_c is the circular speed at the solar radius, $c_\Psi(\odot)$ is the ellipticity of the isopotentials near the Sun, and 2α and p are the exponents of the axisymmetric and nonaxisymmetric components of the potential, respectively (eqs. [2] and [3]). Contours are spaced at $\chi^2 = 1, 2, \ldots, 20$ above the minimum, whose location is indicated by a dot in each panel.

disk might explain the data equally well, though neither this possibility nor the Blitz and Spergel model can account for all the data perfectly. He also concluded that the irregularities seen in the structure of the H I warp at large radii suggest that the outer gas may not be in dynamical equilibrium, in which case the use of this distant gas to probe the potential would be suspect. This notion is supported by strong evidence (see § 4) that on average the distant anticenter stars move *outward* slightly with respect to the LSR, whereas the H I line shows a wing of gas *approaching* us.

In KT, we compared the local observations summarized in § 3 of this paper with the predictions of the Blitz and Spergel model. The comparison is summarized in Table 3. Although the observations are reasonably consistent with the Blitz and Spergel model (except for the vertex deviation, where the prediction differs from the observation by 3.5 times the likely error), a stationary axisymmetric model (or, equivalently, a nonaxisymmetric model with $s_\Psi = 0$), for which all four quantities in the table should be zero, provides a substantially better fit.

The H I emission that led Blitz and Spergel to their conclusion arose from gas at distances beyond $2R_0$. At such large distances there is little evidence to suggest that the gas is in equilibrium. Merrifield's (1992) method also breaks down around this radius, since the observed function $R(W)$ (see § 4.5) is no longer monotonic. We now argue that for $R \lesssim 2R_0$ there is no evidence that favors the Blitz and Spergel model over an axisymmetric one, and that for $R \gtrsim 2R_0$ the gas is not in equilibrium.

In Figure 10 we illustrate the shape of the warp, by plotting the elevation of the Galactic midplane as a function of Galactic azimuth ϕ. Different rings R = constant are plotted, using three different assumptions for the velocity field: (*a*) circular motion for the gas and the LSR, with a common circular speed $v_c = 225$ km s^{-1}; (*b*) the Blitz & Spergel (1991) model, with $v_c = 225$ km s^{-1} and an outward motion of the LSR of 14 km s^{-1}; and (*c*) our best-fit standard model, equation (55). Each vertical column compares rings with the same value of $W_0 \equiv v_c(R_0/R - 1)$ (compare eq. [38]), rather than the same radius R, to help ensure that more or less the same emission is used in the comparison. The calculation is straightforward: for each velocity field, we evaluate the ring radius corresponding to $W_0 = -100$, -120, and -133 km s^{-1}; we then calculate the velocity of points on this ring as a function of longitude, read off the Galactic latitude of the maximum intensity of H I line emission at that velocity from the surveys of Weaver & Williams (1974) and Kerr et al. (1986), and convert this angle into a height above the (inner) Galactic plane. Figure 10 shows that

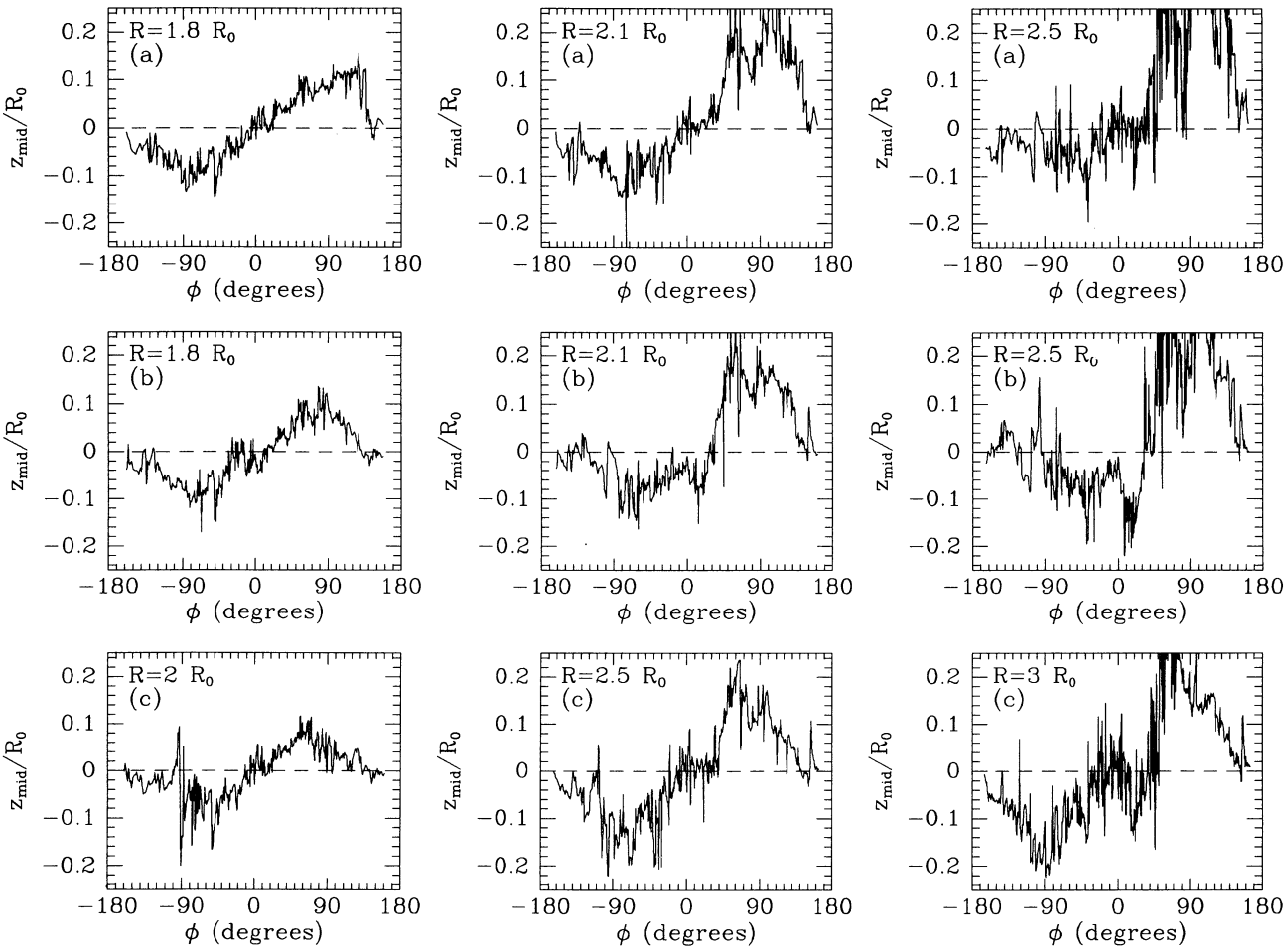

FIG. 10.—Height of rings of constant radius above the Galactic plane for three velocity fields: (*a*) circular motion with speed $v_c = 225$ km s^{-1}; (*b*) the Blitz & Spergel (1991) model, with circular speed $v_c = 225$ km s^{-1} and an outward motion of the LSR of 14 km s^{-1}; (*c*) our best-fit standard model, eq. (55). The radii are chosen so that $W_0 \equiv v_c(R_0/R - 1)$ is the same in each vertical column; since the circular speed is different in case (*c*), the rings in the last row have slightly different radii from the first two rows. In a warped disk composed of tilted rings, which is a good approximation to the expected configuration for a steady state warp, these curves should be sinusoidal.

1. The axisymmetric velocity field (case [*a*], *first row*), implies that the outer gas layer warps quite irregularly, even at radii as small as $R = 1.8R_0$—the midplane curve in the first panel does not have the sinusoidal shape that is required if the gas is in a tilted planar ring. At larger radii the well-known asymmetry of the Galactic warp is very noticeable. It is hard to see how a gas layer of this shape can be in equilibrium.

2. The same irregularity is present if the Blitz and Spergel model is used (case [*b*], *second row*), which is particularly worrisome since this model was derived on the assumption that the horizontal motion of gas at radii as large as $2.3R_0$ is described by closed streamlines.

3. The irregularities, while still present, are reduced in the velocity field of the standard model (case [*c*], *third row*). The outermost gas that has been used in the analysis of this (and Merrifield's) paper ($R \lesssim 2R_0$) appears to lie in a tilted planar ring (the elevation vs. azimuth plot is approximately sinusoidal), consistent with a steady state warp.

Thus, in summary, the shape of constant-radius slices through the gas in the outer Galaxy suggests that the material at $R \gtrsim 2R_0$ is not in an equilibrium steady state, which, if true, erodes much of the evidence for the Blitz-Spergel model. The shape of the gas layer for $R \lesssim 2R_0$ is much closer to the tilted ring characteristic of a steady state warp, especially if the velocity field of the standard model is assumed.

Despite the reassurance provided by Figure 10, it is unsettling for our belief in the standard model that the distribution of distant gas shows no direct evidence of an elliptical distortion: as Blitz and Spergel discuss, the faintest contours of brightness temperature in the (l, v_{los}) diagram do not show the characteristic deviation from sine curves that would be expected of the outer regions of an equilibrium elliptical disk. Perhaps the elliptical distortion decays slowly with radius, or

TABLE 3

COMPARISON OF THE BLITZ-SPERGEL MODEL TO LOCAL OBSERVATIONS

Parameter	Blitz & Spergel	Observed
Oort C (km s^{-1} kpc^{-1})	1.9	0.6 ± 1.1
Oort K (km s^{-1} kpc^{-1})	0.4	-0.35 ± 0.5
Vertex deviation	−9°.3	$5°.5 \pm 4°.2$
LSR v_R (km s^{-1})	14	-1 ± 9

NOTES.—Predictions of the Blitz & Spergel 1991 model, and observed values (KT). The observational errors listed are "likely" errors as defined in § 3.

perhaps the nonequilibrium distribution of gas in the outermost disk obscures the kinematic signature of the ellipticity.

8. THE VELOCITY OF THE LOCAL STANDARD OF REST

In the standard model, with the Sun on a symmetry axis of the potential, the velocity of the LSR is $v_{\rm LSR} = v_c(1 - c_\Psi)$. For our best-fit parameters (eq. [55]), we find $v_{\rm LSR} = 180 \pm 10$ km s^{-1}, much lower than the conventional IAU estimate of 220 km s^{-1}. (For the more general power-law models of eq. [54], we find $v_{\rm LSR} = 172 \pm 17$ km s^{-1}.)[5] We now ask how this substantial revision of $v_{\rm LSR}$ affects our understanding of the dynamics of the Galactic halo and the local Group.

The reduction in $v_{\rm LSR}$ from 220 to 180 km s^{-1} changes the line-of-sight velocity of M31 relative to the Galactic center from -120 to -150 km s^{-1}. The higher infall velocity increases the mass of the Local Group estimated from the timing argument (Kahn & Woltjer 1959; Peebles et al. 1989; Raychaudhury & Lynden-Bell 1989; Kroeker & Carlberg 1991): if the age of the universe is 15 Gyr, the estimated Local Group mass is increased by about 35%, from 3.7×10^{12} to $5.0 \times 10^{12}\ M_\odot$, which is still consistent with plausible models of galaxy formation.

The velocity $v_{\rm LG}$ of the Sun with respect to the barycenter of the Local Group may be estimated from the statistics of the line-of-sight velocities of independent Local Group members, without assuming a value for $v_{\rm LSR}$.[6] We adopt Einasto & Lynden-Bell's (1982) "first" solution, which gives $v_{\rm LG} = 304$ km s^{-1} toward $l = 97°$, $b = -1°$. Assuming that the momenta of the Galaxy and M31 are equal and opposite with respect to the local Group barycenter, which is plausible since they contain most of the stars, this result yields (Einasto & Lynden-Bell 1982, p. 70)

$$M_{\rm A}/M_{\rm G} = 6.45 - 0.02 v_{\rm LSR} = 6.45 - 0.02 v_c(1 - c_\Psi)\,, \quad (56)$$

where $M_{\rm A}$ and $M_{\rm G}$ are the masses of M31 and the Galaxy. Einasto and Lynden-Bell suggest that we use the Tully-Fisher relation[7] to set $M_{\rm G}/M_{\rm A} = (v_c/250\ {\rm km\ s^{-1}})^4$ (assuming identical mass-to-light ratios for M31 and the Galaxy). Together with equation (56), this gives us a relation between v_c and c_Ψ. For an axisymmetric disk, $c_\Psi = 0$, we find $v_c = 200$ km s^{-1}, somewhat lower than the IAU value of 220 km s^{-1}, while for $c_\Psi = 0.08$ we find $v_c = 191$ km s^{-1}, in adequate agreement with our best estimate from disk kinematics, $v_c = 197$ km s^{-1} for $c_\Psi = 0.08$. The errors in this determination are at least ± 30 km s^{-1}, so Local Group kinematics do not provide an accurate way to determine v_c but our result does show that the nonaxisymmetric model that we are advocating is compatible with the observed motion of the Sun relative to the Local Group.

The velocity of the LSR also influences models of the orbits of the Magellanic Clouds and Magellanic Stream (a narrow band of H I gas extending along a great circle arc of $\sim 100°$). The barycenter of the Large and Small Magellanic Clouds is presently 50 kpc from the Galactic center and moving outward (at 68 km s^{-1} if $v_{\rm LSR} = 220$ km s^{-1}, or 100 km s^{-1} if $v_{\rm LSR} = 180$ km s^{-1}), so in most plausible models the Clouds have recently passed pericenter. The Magellanic Stream is believed to consist of tidal debris from the Clouds that was torn off at the prior pericenter passage and is now trailing behind the Clouds (Murai & Fujimoto 1980; Lin & Lynden-Bell 1982). The principal theoretical challenge for models of the Stream is to reproduce the high infall velocity at the tip of the Stream 100° from the Clouds, $v_{\rm tip} = -380$ km s^{-1} $+ 0.82 v_{\rm LSR}$. The high infall velocity requires a highly eccentric orbit for the Clouds, since the gas roughly traces the Clouds' orbit; however, if the eccentricity is too high or the halo potential gradient is too weak, the orbital period of the Clouds becomes so large that the Stream disperses in less than one orbital period.

These considerations are quantified by Lin & Lynden-Bell (1982), who derive $v_c = 244 \pm 12$ km s^{-1} by fitting the Stream kinematics, assuming that the halo is spherical with circular speed v_c, and that $v_{\rm LSR} = v_c$. Our model, with $v_{\rm LSR} = 180$ km s^{-1}, yields a Stream infall velocity $|v_{\rm tip}|$ that is larger by 52 km s^{-1} and requires a more massive halo to generate these larger velocities, perhaps $v_c \approx 340$ km s^{-1} in the region of the Cloud orbit.[8] A halo that is so massive is not excluded by the observations—we have only crude observational constraints on halo potentials at distances $\gtrsim 30$ kpc—and in addition some of the assumptions of these models for the Stream may be incorrect: (1) halos are likely to be strongly triaxial, not spherical; (2) the Stream may be influenced by nongravitational forces; (3) there may be alternative models for the Stream dynamics, for example ones in which the Clouds have just completed their first pericenter passage (Shuter 1992).

The velocity of the LSR is reflected in the motions of globular clusters, halo stars, and satellite galaxies. Determination of $v_{\rm LSR}$ from these tracer populations is complicated by several problems. (1) In some cases (e.g., globular clusters) the tracer population has its own rotation velocity, which is highest for metal-rich tracers but may not vanish even for the most metal-poor subset of the population. (2) The heliocentric line-of-sight velocities of tracers near the Galactic center depend strongly on the systematic rotation of the tracers but are insensitive to $v_{\rm LSR}$, while the velocities of tracers at distances $\gg R_0$ are affected by $v_{\rm LSR}$ but not by rotation. Unfortunately, there are few objects with known velocities at large distances, and such objects may not yet be in a steady state. (3) The halo population may have originated in a few large fragments that have been tidally disrupted but are not yet well-mixed, even in the solar neighborhood. This possibility is supported by the observation that the velocity distribution of metal-weak stars is skewed, both in the wings and near its center (Norris & Ryan 1989). (4) Many samples of halo stars are kinematically biased (e.g., by looking for stars with large proper motion). Such bias discriminates against stars with velocities similar to that of the Sun and hence leads to an overestimate of $v_{\rm LSR}$.

We have collected velocities of 18 objects (globular clusters, dwarf spheroidal galaxies, and the Magellanic Clouds barycenter) at distances between 25 and 230 kpc from the Galactic center (Little & Tremaine 1987; Zaritsky et al. 1989). Assuming that the distribution of Galactocentric velocities of these objects is isotropic (with zero mean) and Gaussian, we

[5] Both these numbers, as well as IAU estimate, are consistent with Backer & Sramek's (1987) measurement of the proper motion 6.0 ± 0.7 milliarcsec yr^{-1} of the radio source Sgr A* at the center of the Galaxy: using $R_0 = 7.5 \pm 0.9$ kpc (§ 4.1) and correcting for the contribution of the solar motion relative to the LSR yields an azimuthal LSR velocity of 198 ± 34 km s^{-1}.

[6] Because $v_{\rm LG}$ is the velocity used to convert heliocentric line-of-sight velocities of extragalactic objects to the Local Group barycenter, revisions of $v_{\rm LSR}$ do not directly affect extragalactic velocity fields such as the Virgocentric flow.

[7] We note in passing that changing v_c as we advocate, from 220 to 200 km s^{-1} substantially affects the Galaxy's position on the Tully-Fisher relation. If the Galaxy were the sole calibrator of this relation (cf. de Vaucouleurs 1983), the change would lower the Hubble constant by 20%.

[8] The number comes from a slight generalization of Lin & Lynden-Bell's (1982, § 5) discussion to the case where $v_c \neq v_{\rm LSR}$, which yields the formula 636 km s^{-1} $- 1.55 v_{\rm LSR} = 1.05 v_c$.

find that the maximum-likelihood estimate of v_{LSR} is 234 km s^{-1}, with 1 σ limits from 187 to 281 km s^{-1}; our preferred value of 180 km s^{-1} is 1.2 σ away from the most likely value. This result is quite sensitive to the selection of satellites; for example, if the galaxies are removed, the remaining 10 globular clusters yield $v_{LSR} = 146$ km s^{-1} with a 1 σ upper limit of 221 km s^{-1}.

We have also estimated v_{LSR} from 25 globular clusters with Galactocentric distances between 10 and 25 kpc (data from Thomas 1989). All but one of these clusters is metal-weak, [Fe/H] < -1. Assuming that the distribution of Galactocentric velocities of these objects is isotropic and Gaussian, we find that the maximum likelihood estimate of v_{LSR} is 188 km s^{-1}, with 1 σ limits of 142 to 235 km s^{-1}.

Many authors have estimated v_{LSR} from samples of halo stars (see reviews by Freeman 1987 and Majewski 1992). The results vary widely and do not provide a strong constraint on v_{LSR}.

Carlberg & Innanen (1987) have argued that samples of high-velocity dispersion disk stars should be depleted near zero angular momentum, because orbits with low angular momentum are chaotic if the Galaxy has a centrally concentrated mass distribution, and hence cannot be confined to a disk. The available data on high-velocity disk stars show a depletion that implies $v_{LSR} = 235 \pm 10$ km s^{-1}, but the statistical significance of the depletion is not very high.

To summarize, we feel that there is no strong evidence from the tests presented in this section that distinguishes between the traditional IAU value for the velocity of the local standard of rest, $v_{LSR} = 220$ km s^{-1}, and the value proposed in this paper, $v_{LSR} = 180$ km s^{-1}.

9. SUMMARY

Modern theories of galaxy formation and observations of other galaxies both suggest that many galaxy disks are likely to be elliptical, with an axis ratio $q < 1$ that may be as small as 0.9.

In analyzing the evidence for ellipticity in our Galaxy, it is useful to work with parameters $c_\Psi = \epsilon_\Psi \cos 2\phi_b$, $s_\Psi = \epsilon_\Psi \sin 2\phi_b$ (eq. [14]), where ϕ_b is the azimuthal angle between the Sun and the minor axis of the equipotential surfaces and $1 - \epsilon_\Psi$ is their axis ratio.

A nonzero value of s_Ψ is manifested by asymmetries in the spatial distribution and kinematics between tracers at longitudes l and $-l$, and by nonzero values of the vertex deviation and the radial velocity of the local standard of rest relative to the Galactic center. We find no consistent evidence for a distortion of this kind (§§ 3.1–3.3), implying either that the disk is axisymmetric ($\epsilon_\Psi \approx 0$) or the Sun is near a symmetry axis ($\sin 2\phi_b \simeq 0$). Nevertheless, there are some indications of nonaxisymmetry with odd symmetry (discussed in § 4): these include an outward motion of stars toward longitude 180° and an asymmetry in the integrated H I flux between positive and negative longitudes. We suspect that these anomalies are not the result of large-scale perturbations to the Galactic potential, but their interpretation remains unclear.

Detection of the component c_Ψ is more difficult. In particular, this perturbation maintains the Galactic symmetry about the $l = 0$, 180° line. Existing velocity surveys of tracers, which extend to distances of order R_0, can be fit equally well by axisymmetric models and by elliptical models with c_Ψ as large as 0.2. However, the rotation curves derived from these surveys are sensitive to c_Ψ: if c_Ψ is 0.1, the rotation curves can be in error by 20% or more (§ 4.4).

We have analyzed a specific model of an elliptical disk, in which the rotation curve is flat and the ellipticity is independent of radius. We focus on two significant anomalies in fitting observations to axisymmetric disk models: (1) The squared axis ratio of the velocity ellipsoid in the solar neighborhood is 0.42 ± 0.06 compared to a predicted value of 0.66 ± 0.06 (§ 3.4); (2) the rotation speed in the range $R = R_0$ to $2R_0$ obtained from the kinematics of Cepheids and carbon stars is roughly 20% higher than the rotation speed derived from the vertical distribution and kinematics of distant H I. Both of these anomalies are removed in elliptical disk models with $c_\Psi \simeq 0.08$; the corresponding rotation speed is roughly constant at 200 km s^{-1} out to $2R_0$ or more (§ 5). From local kinematics sensitive to s_Ψ, we deduce that in such a model the Sun would lie near the minor axis of the potential (equivalently, the major axis of the disk). The velocity of the local standard of rest would be 180 km s^{-1} (§ 8). Our best-fit model is described by equations (55). We have also investigated more general models, in which the rotation curve and the amplitude of the elliptical distortion are power laws in radius, but these do not offer significantly improved fits to the data (§ 6). Generalizations that we have not examined include distortions with other azimuthal wavenumbers or nonzero pattern speeds.

A possible concern with our model is that the kinematics of the outermost H I gas ($R \gtrsim 2R_0$) show no direct evidence of an elliptical distortion of the kind we advocate; however, the interpretation of the behavior of this gas is difficult because it is probably not in a steady state (§ 7).

The alignment of the Sun with the symmetry axis of the elliptical disk is not ad hoc or improbable. The Sun can be as much as $\pm 10°$ off the symmetry axis (§ 3.5) so the a priori probability of the alignment is $20°/90° \simeq 0.2$. Moreover, the Sun-Galactic center line is roughly perpendicular to the line of nodes of the Galactic warp, and if the warp is due to a tilt between the halo and the inner disk then it is plausible that the minor axis of the halo potential in the disk plane should lie along the Sun-center line. In any case, because the effects of the c_Ψ and s_Ψ terms are independent, our conclusions concerning c_Ψ do not rely on the smallness of s_Ψ.

The evidence for the specific values of rotation speed and ellipticity that we advocate here is suggestive but not compelling. Thus our most robust conclusion is that plausible models of the Galaxy, in which the disk is elliptical and the Sun is near a symmetry axis, allow a remarkably wide range of velocities for the Local Standard of Rest. In addition, we have shown that simple elliptical disk models have the capacity to resolve several puzzling features seen in the kinematics of the Galaxy. This success suggests that more sophisticated elliptical models may provide an important tool for interpreting observations of Galactic structure.

We thank James Binney and Leo Blitz for comments on the manuscript. This research was supported in part by an operating grant from NSERC (S. T.), and by a Hubble Fellowship (K. K.) through grant HF-1020.01-91A awarded by the Space Telescope Science Institute (which is operated by the Association of Universities for Research in Astronomy, Inc., for NASA under contract NAS5-26555).

REFERENCES

Backer, D. C., & Sramek, R. A. 1987, in The Galactic Center, ed. D. C. Backer (New York: AIP), 163
Binney, J. 1978, MNRAS, 183, 779
Blitz, L. 1992, in Astrophysical Disks, ed. S. F. Dermott, J. H. Hunter, & R. E. Wilson (New York: New York Acad. Sci.), 151
Blitz, L., & Spergel, D. N. 1991, ApJ, 370, 205
Caldwell, J. A. R., & Coulson, I. M. 1989, in The Outer Galaxy, ed. L. Blitz & F. J. Lockman (Berlin: Springer), 68
Carlberg, R. G., & Innanen, K. A. 1987, AJ, 94, 666
de Vaucouleurs, G. 1983, ApJ, 268, 451
Dubinski, J., & Carlberg, R. G. 1991, ApJ, 378, 496
Einasto, J., & Lynden-Bell, D. 1982, MNRAS, 199, 67
Fich, M., Blitz, L., & Stark, A. A. 1989, ApJ, 342, 272
Franx, M., & de Zeeuw, T. 1992, ApJ, 392, L47
Freeman, K. C. 1987, ARA&A, 25, 603
Gunn, J. E., Knapp, G. R., & Tremaine, S. 1979, AJ, 84, 1181
Gwinn, C. R., Moran, J. M., Reid, M. J., Schneps, M. H., Genzel, R., & Downes, D. 1989, in The Center of the Galaxy, ed. M. Morris (Dordrecht: Kluwer), 47
Kahn, F. D., & Woltjer, L. 1959, ApJ, 130, 705
Katz, N., & Gunn, J. E. 1991, ApJ, 377, 365
Kerr, F. J., & Lynden-Bell, D. 1986, MNRAS, 221, 1023
Kerr, F. J., Bowers, P. F., Jackson, P. D., & Kerr, M. 1986, A&AS, 66, 373
Kormendy, J. 1988, in Origin, Structure and Evolution of Galaxies, ed. L.-Z. Fang (Singapore: World Scientific), 252
Kroeker, T., & Carlberg, R. G. 1991, ApJ, 376, 1
Kuijken, K. 1991, in Warped Disks and Inclined Rings around Galaxies, ed. S. Casertano, P. Sackett, & F. Briggs (Cambridge: Cambridge Univ. Press), 159
Kuijken, K., & Gilmore, G. 1989, MNRAS, 239, 605
Kuijken, K., & Tremaine, S. 1991, in Dynamics of Disk Galaxies, ed. B. Sundelius (Göteborg: Göteborg Univ. Press), 71 (KT)
Lacey, C. 1991, in Dynamics of Disk Galaxies, ed. B. Sundelius (Göteborg: Göteborg Univ. Press), 257
Lewis, J. R., & Freeman, K. C. 1989, AJ, 97, 239
Lin, D. N. C., & Lynden-Bell, D. 1982, MNRAS, 198, 707
Little, B., & Tremaine, S. 1987, ApJ, 320, 493
Majewski, S. R. 1992, ApJS, 78, 87
Merrifield, M. R. 1992, AJ, 103, 1552
Metzger, M. R., & Schechter, P. L. 1993, AJ, submitted
Murai, T., & Fujimoto, M. 1980, PASJ, 32, 581
Norris, J. E., & Ryan, S. G. 1989, ApJ, 336, L17
Peebles, P. J. E., Melott, A. L., Holmes, M. R., & Jiang, L. R. 1989, ApJ, 345, 108
Petrovskaya, I. V., & Teerikorpi, P. 1986, A&A, 163, 39
Radhakrishnan, V., & Sarama, N. V. G. 1980, A&A, 85, 249
Raychaudhury, S., & Lynden-Bell, D. 1989, MNRAS, 240, 195
Reid, M. J. 1989, in The Center of the Galaxy, ed. M. Morris (Dordrecht: Kluwer), 37
Rohlfs, K., Chini, R., Wink, J. E., & Böhme, R. 1986, A&A, 158, 181
Sackett, P. D., & Sparke, L. S. 1990, ApJ, 361, 408
Schechter, P. L., Aaronson, M., Cook, K. H., & Blanco, V. M. 1989, in The Outer Galaxy, ed. L. Blitz & F. J. Lockman (Berlin: Springer), 31
Shuter, W. L. H. 1992, ApJ, 386, 101
Thomas, P. A. 1989, MNRAS, 238, 1319
Weaver, H., & Williams, D. R. W. 1974, A&AS, 17, 1
Zaritsky, D., Olszewski, E. W., Schommer, R. A., Peterson, R. C., & Aaronson, M. 1989, ApJ, 345, 759